

1 **Contrasting biophysical controls on carbon dioxide and methane outgassing from** 2 **streams**

3
4 **L. Rovelli^{1,*}, L. A. Olde^{2,‡}, C. M. Heppell³, A. Binley⁴, G. Yvon-Durocher⁵, R. N. Glud^{6,7,}**
5 **⁸ and M. Trimmer^{2,*}**

6
7 ¹iES - Institute for Environmental Sciences, University of Koblenz-Landau, 76829 Landau,
8 Germany.

9 ²School of Biological & Chemical Sciences, Queen Mary University of London, London E1
10 4NS, United Kingdom.

11 ³School of Geography, Queen Mary University of London, London E1 4NS, United
12 Kingdom.

13 ⁴Lancaster Environment Centre, Lancaster University, Lancaster, LA1 4YQ, United
14 Kingdom.

15 ⁵Environment and Sustainability Institute, University of Exeter, Penryn, Cornwall, TR10
16 9EZ, United Kingdom.

17 ⁶HADAL & Nordcee, University of Southern Denmark, 5230 Odense M, Denmark.

18 ⁷Danish Institute of Advanced Study – DIAS, University of Southern Denmark, 5230 Odense
19 M, Denmark.

20 ⁸Department of Ocean and Environmental Sciences, Tokyo University of Marine Science and
21 Technology, 108-8477 Tokyo, Japan.

22
23 * Corresponding authors: Mark Trimmer (m.trimmer@qmul.ac.uk) and Lorenzo Rovelli
24 (rovelli@uni-landau.de)

25 ‡ now at Rothamsted Research, West Common, Harpenden, AL5 2JQ, United Kingdom.

26 27 **Key Points:**

- 28 • There are different controls on the outgassing of the greenhouse gases carbon dioxide
29 and methane in streams.
- 30 • Carbon dioxide results largely from physical run-off from the land and is then altered
31 in stream by biology depending on season.
- 32 • In contrast, methane is created in the streambed but once released to the stream is then
33 dissipated by the physical forces of stream flow.

34

35 Abstract

36 Small headwater streams are recognized for intense outgassing to the atmosphere of
37 climate-relevant carbon dioxide (CO₂) and methane (CH₄). Though these headwaters are
38 markedly oversaturated for both CO₂ and CH₄, the origins and controls over the fate of these
39 two carbon-gases are still poorly constrained, especially for the stronger greenhouse gas CH₄.
40 Here, by measuring stream-based production of CO₂ and CH₄, concurrently with their rates of
41 outgassing to the atmosphere, we identify distinct biophysical control mechanisms for each
42 gas. We show that while CO₂ is largely imported from the catchment in proportion to discharge,
43 CO₂ outgassing can be modulated by in-stream metabolism to offset outgassing by up to 30%
44 in spring and summer. In contrast, CH₄ shows a non-linear response to seasonal changes in
45 discharge and is predominantly produced in the streambed in relation to sediment type. Further,
46 once released from the streambed, outgassing of CH₄ at the surface and flow-driven dilution
47 occur far more rapidly than biological methane oxidation and CH₄ leaves the water largely
48 unaltered by biology. Incorporating the intense carbon cycling of headwater streams into the
49 global carbon cycle will require distinct parameterizations for each carbon gas in Earth system
50 models.

51

52 Plain Language Summary

53 There is growing interest in the global carbon cycle and how carbon is transformed in the
54 landscape into the greenhouse gases carbon dioxide (CO₂) and methane – with methane being
55 by far the more potent than CO₂. Streams and rivers are recognized hotspots of carbon
56 cycling in the landscape, commonly harboring large amounts of CO₂ and methane – yet what
57 controls either gas in streams is not fully understood. Without that understanding, we cannot
58 predict how carbon cycling will respond to climate change or to other human alteration of the
59 landscape. Here we researched different components of the carbon cycle in streams to show
60 that each gas is influenced by quite distinct “biophysical” control mechanisms. While CO₂ in
61 streams results largely from physical run-off from the land, once in a stream it can be
62 changed by the stream biology that ebbs and flows with the seasons. Contrastingly, methane
63 is largely created by biology within the streambed itself but once released into the wider
64 stream that methane is then dissipated by the physical forces of stream flow. Put more

65 simply, CO₂ is physically carried to the stream to then be altered by biology, whereas as
66 methane is borne from biology in the stream, to then be physically carried away.

67 **1 Introduction**

68 Rivers and streams transport, store and transform large quantities of carbon (Battin et
69 al., 2009; Cole et al., 2007) and are routinely supersaturated with the two climatically
70 important carbon gases methane (CH₄) and carbon dioxide (CO₂) which they outgas to the
71 atmosphere (Raymond et al., 2013; Stanley et al., 2016). Small headwater streams (<20 km²
72 catchment area) consistently have the highest oversaturation for CO₂ and, despite their small
73 extent, contribute some 36% (i.e., 0.93 Pg C yr⁻¹) of the total CO₂ outgassing from river
74 networks globally (Marx et al., 2017). In contrast, headwater streams appear no more
75 saturated in CH₄ than larger rivers and estimated CH₄ outgassing rates are similar across
76 streams and rivers of comparable sizes (Stanley et al., 2016). Hence, the origins and fate of
77 these two important carbon gases in headwater streams appear different. While we
78 understand more about CO₂ compared to CH₄ in rivers and streams (Stanley et al., 2016) in
79 general, the origins and final fates of both carbon gases remain poorly constrained (Crawford
80 & Stanley, 2016; Striegl et al., 2012).

81 The supersaturation and subsequent outgassing of CO₂ and CH₄ throughout river
82 networks can be due to both carbon metabolism in the bed and gases imported from the
83 catchment (Butman & Raymond, 2011; Crawford & Stanley, 2016; Jones & Mulholland,
84 1998b; Peter et al., 2014; Sanders et al., 2007; Striegl et al., 2012), including weathering for
85 CO₂. For CO₂, terrestrial inputs can be the dominant source of CO₂ emitted from the river
86 (Butman & Raymond, 2011; Striegl et al., 2012), though the magnitude of this component is
87 dependent on river and stream size and seasonal changes in discharge (Hotchkiss et al.,
88 2015). Before CO₂ is finally outgassed, there can be further modulation by net ecosystem
89 production depending on season and diel cycle (Lynch et al., 2010; Peter et al., 2014; Reiman
90 & Xu, 2018; Rocher-Ros et al., 2020; Stets et al., 2017), but these biological dynamics have
91 not been quantified directly and remain essentially unknown for CH₄.

92 Despite the relative paucity of data for CH₄ in rivers and streams, their estimated total
93 annual outgassing has recently been revised upwards from 1.5 Tg CH₄ yr⁻¹ in 2011 (see
94 Bastviken et al., 2011), to 26.8 Tg CH₄ yr⁻¹ in 2016 (Stanley et al., 2016) and 30.3 Tg CH₄ yr⁻¹
95 in 2021 (Li et al., 2021) which highlights the growing evidence for the significance of
96 running waters in the global CH₄ budget. For example, the recent revision increases the total
97 contribution from rivers, streams and lakes to global CH₄ emissions from 40 Tg CH₄ yr⁻¹, to
98 70.3 Tg CH₄ yr⁻¹, which is equivalent to 32% of that emitted from wetlands (217 Tg CH₄ yr⁻¹;

99 Ciais et al., 2013). As CH₄ is a far more potent greenhouse gas than CO₂ (Myhre et al., 2013),
100 the partitioning between either carbon gas emitted from rivers and streams is particularly
101 relevant to climate forecasting. In addition, anthropogenic land use change and habitat
102 destruction are likely to have a relatively greater influence on riverine CH₄ dynamics
103 (Crawford & Stanley, 2016; Sanders et al., 2007; Yu et al., 2017), compared to CO₂. Despite
104 these concerns, our understanding of the contemporaneous biophysical controls of these two
105 carbon gases in rivers and streams in general is still lacking (Jones & Mulholland, 1998b; Yu
106 et al., 2017).

107 The aim of this study was to characterize how discharge and in-stream carbon
108 metabolism together exert biophysical controls on the sources and final fates of CO₂ and CH₄
109 in temperate, low-gradient headwater streams (maximum catchment area of ~60 km²) in our
110 case study catchment of the lowland Hampshire River Avon, UK. Within the catchment, we
111 performed a seasonal study on six streams with distinct geologies (two each on the clay,
112 Greensand and Chalk) and over a wide spectrum of hydrological characteristics, e.g., flashy
113 to stable hydrograph, hydrological connectivity to the land and in-stream carbon metabolism
114 (see Heppell et al., 2017; Rovelli et al., 2017, 2018). To quantify how much outgassing of
115 CO₂ and CH₄ could be accounted for by either in-stream production or input from the
116 catchment, we combined: i) traditional measurements of benthic metabolism via isolated
117 benthic chambers (Trimmer et al., 2009) with; ii) integrated estimates of whole stream
118 metabolism using the state-of-the-art and non-invasive aquatic eddy covariance technique
119 (Rovelli et al., 2017, 2018); and iii) direct quantification of CO₂ and CH₄ outgassing from
120 anchored floating chambers (Podgrajsek et al., 2014) (see Figure 1). The seasonal study was
121 complemented by measurements of CO₂ and CH₄ concentrations in riparian soils and
122 streambeds and laboratory-based assessments of the potential for methane oxidation in the
123 water column. Finally, we made high-temporal-resolution day and night measurements of
124 CO₂ and CH₄ outgassing and modeled any diel changes as functions of our directly
125 parameterized biological (e.g., net ecosystem metabolism, water column methane oxidation)
126 and physical control mechanisms (e.g., dilution, reaeration, outgassing).

127

128 **2 Materials and Methods**

129 2.1 Study site

130 This study was performed in six ~150 m headwater reaches of the lowland catchment
131 of the Hampshire River Avon (UK) (Figure 1a; Allen et al., 2014; Jarvie et al., 2005). The
132 headwaters drain three dominant geologies: Chalk (River Ebble and River Wylye), (Upper)
133 Greensand, i.e., fine-grained glauconitic sands and sandstones, (River Nadder and West
134 Avon) and clay (River Sem and Priors), although some sub-catchments and reaches
135 encompass a combination of those geologies, e.g., clay and Greensand on River Nadder,
136 Chalk and Greensand on River Wylye (Figure 1a). Here, we regard these sub-catchments
137 based on their dominant underlying geology, which has been shown to modulate the local
138 hydrology and hydrological connectivity (Bristow et al., 1999). Parallel studies at these
139 reaches have also directly linked hydrological regime and baseflow index (BFI) to the
140 dynamics of key stream sediment processes such as nitrogen gas (N₂) production (Lansdown
141 et al., 2016), and nutrient dynamics (Heppell et al., 2017). Integrated baseflow, as a
142 proportion of total flow over a single day, has also been identified as a robust predictor of
143 seasonal differences in stream metabolism dynamics across the different reaches (Rovelli et
144 al., 2017). The water column of these lowland headwaters has been shown to contribute to
145 about a quarter of their annual whole-stream respiration and primary production, with water
146 column respiration in the turbid waters, e.g. River Sem on the clay, contributing, on average,
147 71.3% of the spring and summer whole-stream respiration (Rovelli et al., 2017, 2018).
148 Surface water sampling by Heppell et al. (2016a) has shown that mean pH remained largely
149 comparable across the sites ranging from 7.3 to 7.7, although with the clay streams tending
150 towards lower values. In contrast, mean dissolved inorganic carbon (DIC) was, on average,
151 highest in the Chalk streams and in the Greensand West Avon (3.9 to 4.8 mmol L⁻¹) and
152 lowest in Greensand Nadder and in the clay streams (3.0 to 3.1 mmol L⁻¹). Estimates of total
153 alkalinity based on pH and DIC (after Millero, 1979) were in the order of 2650 to 2900 μmol
154 L⁻¹ (clay streams and Nadder) and 3600 to 4520 μmol L⁻¹ (chalk streams and West Avon),
155 respectively.

156 For the purposes of this study, each reach was studied for a period of one to three days
157 in spring, summer, autumn and winter from April, 2013, until February, 2014. Using a variety
158 of techniques (Figure 1), we quantified fluxes of dissolved oxygen (O₂), carbon dioxide
159 (CO₂) and methane (CH₄) using chambers (benthic and floating) and O₂ fluxes via aquatic

160 eddy covariance (Rovelli et al., 2017, 2018), along with stream morphological characteristics
161 and local hydrological regime (Heppell et al., 2017). We experienced from below average
162 rainfall in both spring and summer, to a 100-year flood in the winter of 2013 to 2014 and
163 while this allowed us to capture a wide range of stream discharges it was not possible to
164 sample during the extreme flood (see Figures S1, S2). We used piezometers to measure
165 porewater concentrations of CH₄ and CO₂ in riparian soils and streambed sediments every
166 two months (Heppell et al., 2017). A high-resolution survey of day and night CO₂ and CH₄
167 outgassing was performed in spring, 2015, using an automated floating gas chamber
168 connected to an Ultraportable Greenhouse Gas Analyzer (UGGA; Los Gatos Research,
169 California, USA). Benthic mapping surveys were also performed in each reach for each
170 season to characterize the areal coverage of vegetated and non-vegetated patches of clay,
171 Greensand and Chalk gravel following the methods described in Gurnell et al. (1996). The
172 patch type areas were drawn manually onto local geo-referenced stream maps, and were
173 digitized using Adobe Photoshop® to extract relative areal coverage (in percentage) of each
174 sediment patch-type.

175 2.2 Benthic metabolism and sediment CH₄ release.

176 Measurements of *in situ* O₂-based benthic metabolism, along with release of CH₄,
177 were performed at the patch scale (<1 m²) using benthic chambers (Figure 1b; Trimmer et al.,
178 2009). These consisted of transparent Perspex chambers (0.5 L enclosed volume, 73 cm²
179 surface area) mounted on a steel-ring, which were used to measure net benthic O₂ production
180 and CH₄ release in the light ($n = 12$, daytime), and equally-sized black, plastic chambers to
181 measure benthic O₂ consumption and CH₄ release in the dark ($n = 12$, night-time). Potassium
182 chloride was added as a tracer to quantify potential exchange of water from the chamber in
183 the permeable sand and gravel-Chalk beds. The chamber incubations covered the range of
184 sediment patch types identified during the initial stream habitat mapping. Each chamber
185 deployment lasted ~2 hours, and four chambers were deployed each day/night over three
186 successive days. The chambers were continuously stirred using a magnetic stirrer. Changes in
187 O₂ concentration within the benthic chamber were monitored at one-minute intervals using
188 Clark-type oxygen microelectrodes connected to an Under-Water Meter (Unisense, Denmark)
189 (Trimmer et al., 2010). Water samples for CH₄ analysis were taken from the chamber at the

190 beginning and end of each deployment using a syringe connected to a valve on top of the
191 chambers (Figure 1b).

192 Samples for CH₄ were transferred gently to 12mL gas-tight vials (Exetainers, Labco,
193 UK), overfilled to ensure no air was introduced, and preserved within two hours of being
194 taken by adding 100µl zinc chloride solution (7M; see Dalsgaard et al., 2000). CH₄ was
195 measured after headspace equilibration using a gas chromatograph fitted with a flame
196 ionization detector (Agilent Technologies, UK) and concentrations calculated using solubility
197 coefficients (Yamamoto et al., 1976) following established protocols (e.g., Sanders et al.,
198 2007). Rates of O₂ consumption or production over time were calculated using linear-
199 regression and scaled to an areal flux (in mmol m⁻² h⁻¹) using the chamber inner dimensions.
200 Similarly, CH₄ consumption or production rates were calculated using the concentration at
201 the start and end of each deployment. Final rates of benthic gas exchange were scaled-up to
202 the reach using our benthic mapping of each sediment patch type (vegetated, clay, Greensand
203 and Chalk gravel), by weighting the respective patch-averaged rates by the relative areal
204 coverage (in percentage) of each sediment patch-type within the reach. Benthic O₂ exchange
205 was used to estimate reach-scale benthic ecosystem respiration (ER, as mmol CO₂ produced
206 per m⁻² h⁻¹), benthic gross primary production (GPP, as mmol CO₂ consumed per m⁻² h⁻¹) and
207 net benthic ecosystem metabolism (in mmol CO₂ m⁻² h⁻¹) assuming a 1 to 1 ratio for O₂ to
208 CO₂ (Glud, 2008). It is well established that this ratio may vary over the diel cycle, across
209 seasons as well as spatially, within a commonly reported range of 0.8 to 1.2 (e.g., Glud, 2008;
210 Therkildsen & Lomstein, 1993). As changes in the ratio will proportionally affect our rates,
211 these are to be considered conservative estimates. Throughout the manuscript, positive CO₂
212 net benthic metabolism will be used to indicate a release of CO₂ from the benthic
213 compartment into the water column, i.e., a net source of CO₂. The mean benthic gas exchange
214 from each sediment patch type across all sites was estimated by data clustering following a
215 signed logarithmic transform (see Section 2.7).

216 2.3 Seasonal outgassing of CO₂ and CH₄.

217 Outgassing of CO₂ and CH₄ was quantified using anchored floating chambers (8.6 L
218 volume and 674 cm² surface area; Figure 1c) which were deployed in parallel to the benthic
219 chambers (Podgrajsek et al., 2014). The floating chambers consisted of an inverted plastic
220 bowl covered in reflective aluminum tape, fitted with a polyurethane tubing sample port to
221 allow for gas-sampling via a three-way luer-lock valve and a CO₂ sensor (SenseAir; Delsbo,

222 Sweden) (Bastviken et al., 2015). Typical chamber deployments lasted two hours and were
223 performed in the morning, with the CO₂ sensor set to measure at 5-minute intervals. For CH₄,
224 discrete gas samples were taken at regular intervals from the sample port using a gas-tight
225 syringe (SGE International Pty Ltd, Australia) and stored for later analysis by displacing de-
226 gassed, de-ionised water from 3mL gas-tight vials (Exetainers, Labco, UK). Gas samples
227 were analyzed by GC-FID for CH₄ as described above. For each chamber deployment the
228 initial period of linear rise in gas was identified and the change in concentration over this
229 period was converted into outgassing rates using linear regression and the chamber's
230 dimensions. Positive outgassing rates indicate an upward exchange from the streams into the
231 atmosphere, i.e., a net atmospheric source, while negative rates indicate a downward
232 exchange from the atmosphere into the stream system, i.e., a net atmospheric sink. It should
233 be also noted that anchored floating chambers, compared to freely-drifting chambers, might
234 enhance near-surface turbulence and thus bias outgassing rates (Lorke et al., 2015). Although
235 such bias can be substantial in fast flowing, high-gradient streams, flows in our low-gradient
236 streams (Rovelli et al., 2017, 2018) fell below this threshold (see Lorke et al., 2015).

237

238 2.4 High-temporal-resolution diel measurements of CO₂ and CH₄ outgassing (spring 2015).

239 The seasonal outgassing measurements were complemented by an intensive campaign
240 in spring 2015, to characterize short-term outgassing dynamics in each stream. A LiCor
241 Long-Term Chamber (Model 8100-101; LiCor, Nebraska, USA, with a volume of 4.093 L
242 and a surface area of 318 cm²) was modified to float on the streams by mounting it on a
243 plastic cylinder (collar) and life-ring (Figure 1c) and with a total volume (chamber + collar)
244 of 6.29 L. The chamber was connected to a CR800-Series Datalogger (Cambell Scientific
245 Inc, Utah, USA) to control the motorized chamber. During the deployment, the chamber was
246 set to alternately open and close every 10 minutes to flush the chamber and prevent it from
247 equilibrating with the underlying water. Concentrations of CO₂, CH₄ and water vapor were
248 measured at 10 second intervals with an Ultraportable Greenhouse Gas Analyzer (Los Gatos
249 Research, California, USA), attached to the chamber by a closed-loop (Figure 1d). Gas
250 fluxes, corrected for water vapor dilution, that accounted for the opening and closing of the
251 chamber, were computed for each of the consecutive 10 minute closed-chamber intervals
252 using self-written R (R Core Team, 2014) and Matlab[®] scripts. An r² value of 0.9 was used as
253 quality cut-off to flag weak regressions.

254 We also characterized methane ebullition events by analyzing the distribution of the
255 rates of change in CH₄ (in ppm s⁻¹) during all 1416 measurements. Here we ascribed any
256 sharp episodic increase in CH₄ concentration (i.e., sharp peaks increases, see Figure S9) that
257 lasted for at least two or more consecutive data points to an ebullition event and delineated
258 those from steady, diffusional increases in CH₄ (Figure S9). We found that a 5-fold peak
259 increase in the rate of change over the diffusional rate of increase, was the optimal threshold
260 to identify ebullition events. Once identified, these events were subsequently cross-checked
261 against the parallel CO₂ readings to discriminate between ebullition and other non-steady
262 state fluxes or deployment issues (e.g., inadequate sealing, suboptimal flushing of the
263 chamber), which would also result in clear deviation from a linear change in CO₂. The
264 significance of ebullition was quantified in terms of numbers of ebullition events, as well as
265 the overall contribution from ebullition to CH₄ outgassing (single measurements and mean).
266 The latter was estimated as the total rate of CH₄ outgassing (diffusion + ebullition), by
267 computing a point-to-point slope from the first point at the beginning of the (diffusive) linear
268 slope, before an ebullition event, and the last point of the linear slope after an ebullition event
269 (see Figure S9).

270

271 2.5 Whole stream carbon metabolism.

272 An integrative assessment of whole-stream benthic metabolism in each stream was
273 obtained seasonally using the non-invasive aquatic eddy covariance technique (Berg et al.,
274 2003). Aquatic eddy covariance measurements in rivers and streams quantify the dynamics
275 and driving forces of benthic stream metabolism and riverine O₂ gas exchange (Berg et al.,
276 2003; Berg & Pace, 2017; Koopmans & Berg, 2015; Murniati et al., 2015; Rovelli et al.,
277 2017, 2018). In essence, the technique relies on the simultaneous acquisition of high-
278 resolution time series (64 Hz) of both vertical flow velocity and dissolved O₂ concentrations
279 at the same point in the water above the sediment from which turbulence-driven fluctuations
280 in both vertical velocity and O₂ can be extracted. With the appropriate setup and procedures
281 (see Berg et al., 2003; Lorrain et al., 2010; Rovelli et al., 2017, 2018), the co-variance of those
282 fluctuations provides instantaneous O₂ flux estimates that are then averaged over time (e.g.,
283 hours or days) to provide a net estimate of O₂ uptake or release from the sediment. Model
284 validations of the aquatic eddy covariance have shown that the obtained O₂ flux integrates
285 contributions from a theoretically constrained area of the sediment, termed the footprint area,

286 whose extent depends on: i) the distance from the sediment in which the measurements are
287 collected; and ii) specific characteristics of the sediment surface roughness (i.e., bottom
288 roughness length scale) (see Berg et al., 2007). The aquatic eddy covariance technique may
289 capture benthic O₂ fluxes over much larger areas of the streambed (tens of m² footprint) and
290 was, therefore, complimentary to the patch-scale measurements made with the benthic
291 chambers (described above).

292 Our aquatic eddy covariance system consisted of an acoustic Doppler velocimeter
293 (Vector, Nortek A/S, Rud, Norway), Clark-type O₂ microelectrodes (Revsbech, 1989) and
294 submersible amplifiers (McGinnis et al., 2011) and was operated as described in McGinnis et
295 al. (2016) (Figure 1e). Aquatic eddy covariance was used to quantify benthic GPP, ER and
296 net benthic metabolism, while light and dark incubations of discrete water samples (Rovelli et
297 al., 2017, 2018) captured the same parameters in the water to enable us to quantify net, whole
298 stream metabolism (NWM) within each stream reach. This includes contributions from the
299 sediments, water column and aquatic plants to integrate in-stream metabolism at the reach
300 scale (20 to 70 m²). Measurements were made over at least two and half of the three day
301 sampling period at each site. A comprehensive description of the seasonal aquatic eddy
302 covariance work performed within River Sem, River Nadder and River Wylye, as well as
303 Ebble and West Avon in spring, is presented elsewhere (Rovelli et al., 2017, 2018, 2016).
304 Within the remit of this study, we only report the O₂-based net whole-stream metabolism (in
305 mmol m⁻² h⁻¹ or mmol m⁻² d⁻¹) as CO₂, assuming a 1 to 1 ratio of O₂ to CO₂ for metabolic
306 activity (see section 2.2.). As for the benthic chambers, positive net whole-stream metabolism
307 indicates a net release of CO₂ from the benthic compartment into the water column, while
308 negative values indicate a net benthic uptake of CO₂.

309 2.6 Water column oxidation and dilution of streambed CH₄.

310 Estimates of water column methane oxidation rate potentials were obtained for each
311 stream from laboratory-based measurements of methane oxidation rate potentials of
312 suspended particulate matter (SPM, in mg L⁻¹), scaled to *in situ* suspended particulate matter
313 and CH₄ concentrations, following Shelley et al. (2014, 2015). For each site, methane
314 oxidation was measured at a standard CH₄ concentration of 8 μmol L⁻¹ with 100%, 62.5%,
315 37.5% and 0% of the original suspended particulate matter concentration. Gas samples were
316 taken from the headspace at five time points over the incubation period (0 h, 26.5 h, 49 h,
317 122.5 h, and 168 h, respectively) and measured as above and an empirical relationship

318 between suspended particulate matter and methane oxidation derived (Figure S4). Rates of
 319 methane oxidation (in $\text{nmol CH}_4 \text{ g}^{-1} \text{ SPM h}^{-1}$) were obtained via linear regression and
 320 subsequently scaled from the standard laboratory concentration ($C_{\text{stand}} = 8 \mu\text{mol CH}_4 \text{ L}^{-1}$) to
 321 *in situ* CH_4 concentrations ($C_{\text{in situ}}$) using our previously, laboratory established empirical
 322 Michaelis–Menten kinetic relationship between methane oxidation rate (MO) and CH_4
 323 concentration (~ 0.01 to $22 \mu\text{mol L}^{-1}$) for fine sediment (Shelley et al., 2015):

$$324 \quad MO(C_{\text{in situ}}) = V_{\text{max}} C_{\text{in situ}} / (K_m + C_{\text{in situ}}) \quad \text{equation (1)}$$

325 with the maximum rate (V_{max}) equal to $586 \text{ nmol CH}_4 \text{ g}^{-1} \text{ h}^{-1}$ and the Michaelis constant (K_m)
 326 being $3.7 \mu\text{mol L}^{-1}$ for C_{stand} between ~ 0.01 to $22 \mu\text{mol CH}_4 \text{ L}^{-1}$. Background CH_4
 327 concentrations for each stream were obtained from the initial measurements at the beginning
 328 of each benthic chamber incubation (t_0). The potential for methane oxidation associated with
 329 stream-water suspended particulate matter to alter CH_4 concentrations in the water column
 330 was calculated using the methane oxidation rates and the *in situ* ratio of CH_4 concentration to
 331 suspended particulate matter for each stream. The resulting parameter, here termed, Rk_{CH_4} (in
 332 h^{-1}) represents a measure of the turnover time for CH_4 in the water column due to biological
 333 activity. The residence time of CH_4 due to outgassing, here quantified as the reaeration
 334 constant for K_{CH_4} (in h^{-1}), was obtained from standardized gas transfer velocities (k_{600} , in m d^{-1})
 335 estimated for each stream using hydraulic equations (see Section 2.7), accounting for mean
 336 water depths and the Schmidt number for CH_4 at *in situ* stream temperatures (Raymond et al.,
 337 2012). Flow driven dilution of CH_4 , here termed K_{flow} , was defined as the residence time of
 338 water (in h^{-1}) within any stream reach driven by local discharge. A comparison of the ratios
 339 between these parameters enables an assessment of their relative importance in modulating
 340 water column CH_4 dynamics. For instance, a ratio of Rk_{CH_4} to K_{CH_4} or K_{flow} close to 1 would
 341 indicate that microbial, methane oxidation is a major driver of changes in water column CH_4
 342 concentrations.

343 2.7 Mass-balance of diel CO_2 and CH_4 dynamics.

344 The obtained fluxes and field measurements were combined into a simple mass-
 345 balance model to further investigate potential controls on diel changes in dissolved CO_2 and
 346 CH_4 concentration dynamics at the reach scale. Here, concentration changes of CO_2 and CH_4
 347 over time (dC/dt , in $\text{mmol m}^{-3} \text{ h}^{-1}$) were modeled based on: (i) the amount of dissolved gas
 348 coming into the reach from upstream, including from the catchment (F_{in}); (ii) the net gas
 349 release or uptake across the entire streambed surface area of the reach ($F_{\text{streambed}}$); (iii) net

350 biology-mediated gas production or consumption within the water column as it moves
 351 through the reach ($F_{\text{water column}}$); (iv) the net amount of outgassing to the atmosphere occurring
 352 across the entire water surface area of the reach ($F_{\text{outgassing}}$); and (v) the amount of dissolved
 353 gas being discharged downstream at the lower end of the reach (F_{out}) as:

$$354 \quad \frac{dC}{dt} = F_{\text{in}} + F_{\text{streambed}} + F_{\text{water column}} - \frac{A}{V} F_{\text{outgassing}} - F_{\text{out}} \quad \text{equation (2)}$$

355 In Equation 2, F_{in} (in $\text{mmol m}^{-3} \text{h}^{-1}$) is quantified as the dissolved gas concentration upstream
 356 of the reach (C_{upstream} , in mmol m^{-3}) multiplied by water discharge ($\text{m}^3 \text{h}^{-1}$) at the upper end of
 357 the reach, which were both assumed constant throughout the model run. Similarly, F_{out} (in
 358 $\text{mmol m}^{-3} \text{h}^{-1}$) was computed at each time step as the final modeled stream concentration
 359 from equation 2, for the previous time step, multiplied by the discharge out of the reach,
 360 starting from $C_{\text{background}}$ ($t = 0$, in mmol m^{-3}). The model was run for up to 6 h with time steps
 361 of 5 s and a control volume (V) of mean stream width x 150 m length (along the flow
 362 direction) x mean stream depth (in m), assuming a constant stage (i.e., water level). The
 363 model focuses on the difference in CO_2 and CH_4 dynamics between day and night and we
 364 assume a constant rate of supply or loss of these gases from each pathway over the model
 365 run. The modeled mass balance does not include lateral and vertical groundwater recharge
 366 and discharge, respectively, which we know to be comparatively minor on the modeled time
 367 scales (e.g., Rovelli et al., 2018). Water column gas concentrations in the reach come from
 368 field measurements during summer, 2013, and were used for both the initial ($t = 0$)
 369 concentration within the reach ($C_{\text{background}}$, in mmol m^{-3}) and C_{upstream} . For CO_2 , $F_{\text{streambed}}$ (in
 370 $\text{mmol m}^{-3} \text{h}^{-1}$) is the day and night aquatic eddy covariance O_2 -flux (in $\text{mmol m}^{-2} \text{h}^{-1}$)
 371 multiplied by the area-to-volume (A/V) ratio of the control volume, while $F_{\text{water column}}$ (in
 372 $\text{mmol m}^{-3} \text{h}^{-1}$) is the O_2 -flux in bottle incubations with both expressed as CO_2 equivalents
 373 using a 1 to 1 molar ratio as above (Rovelli et al., 2017). These were chosen over invasive
 374 chamber-based fluxes as they are, overall, expected to provide more accurate estimates of
 375 daytime primary production, and more constrained benthic uptake rates in permeable
 376 sediments (e.g., Attard et al., 2015). For CH_4 , $F_{\text{streambed}}$ is the measured sediment CH_4 release,
 377 obtained from the light or dark benthic chambers (in $\text{mmol m}^{-2} \text{h}^{-1}$) multiplied by A/V, while
 378 the suspended particulate matter-scaled methane oxidation rates, in $\text{mmol m}^{-3} \text{h}^{-1}$, were used
 379 for $F_{\text{water column}}$. Positive values of $F_{\text{water column}}$ and $F_{\text{streambed}}$ indicate a source of CO_2 and CH_4
 380 within the water column or a net gas exchange from the benthic compartment into the water

381 column, respectively. Reach-scale outgassing (in $\text{mmol m}^{-2} \text{h}^{-1}$) for both CO_2 and CH_4 was
 382 quantified as:

$$383 \quad F_{outgassing} = -[k(C_{sat} - C)] \quad \text{equation (3)}$$

384 from gas concentrations in the streams (C) and equilibrated atmospheric concentrations (C_{sat})
 385 (Weiss, 1974; Wiesenburg & Guinasso, 1979), with positive values indicating a net
 386 atmospheric source, i.e., a net gas exchange from the stream into the atmosphere. Gas transfer
 387 velocities (k , m h^{-1}) were obtained from k_{600} values scaled by the respective Schmidt numbers
 388 for each gas at in situ water temperature (Raymond et al., 2012). Values of k_{600} were
 389 quantified from stream discharge and site-specific hydraulic parameters, based on the average
 390 output from the seven model parametrizations provided by Raymond et al. (2012), which
 391 were validated previously for two of the investigated streams (see Rovelli et al., 2018).
 392 Temperature time series were obtained from Heppell & Parker (2018).

393 The model requires meaningful estimates of the average day and night benthic CH_4 fluxes for
 394 the dominant streambed patches e.g., vegetated and non-vegetated sand and Chalk gravel, as
 395 well as for clay. Due to the limited amount of data and the inherent heterogeneity of benthic
 396 CH_4 flux measurements, values tended to span several orders of magnitude and were often
 397 characterized by a strong skewness towards higher values (Fig. 2). To minimize the risk of
 398 biasing our mean estimates, the data were transformed as $y = \text{sign}(x) \times \ln(|x| + 1)$ to ensure
 399 that the original sign of the flux would be maintained. The transformed data were then
 400 averaged into clusters in full digit increments (e.g., -1 to 0, 0 to 1, ...) to give each cluster
 401 equal weighting. The resulting monotonic dataset was subsequently averaged, and the
 402 obtained averaged value ($\ln_average$) converted back a mean flux as $F_{mean} \approx$
 403 $\text{sign}(\ln_average) \times e^{|\ln_average|}$. Note that the flux dataset for the gravel patch type were
 404 found to be more constrained than for the other patch types, with 75% of the data falling
 405 within the -0.9 to $1.3 \mu\text{mol m}^{-2} \text{h}^{-1}$ range, and the outliers deviating by a factor of 3 to more
 406 than 600. Given the reduced magnitude of the flux range, the data were averaged
 407 arithmetically.

408 The model was first used to reproduce the CO_2 dynamics, matching the observed
 409 daytime outgassing by fine-tuning both the stream discharge and background CO_2 and CH_4
 410 concentrations to within the range provided by the field observations, e.g., mean, median for
 411 the month (Heppell & Binley, 2016a, 2016b; Rovelli et al., 2017). Model performance was

412 evaluated by comparing the resulting modeled night-time outgassing rates, with the mean
413 values obtained during our high-resolution sampling campaign. The same hydrological
414 parameters, once validated for CO₂, were then applied to CH₄, where the fine-tuning of the
415 model was only performed on the background concentrations. The model was also used to
416 investigate the relevance of different physical and biology-mediated parameters in driving
417 diel changes in CO₂ and CH₄ outgassing, via a measurements-oriented sensitivity analysis.
418 This included discharge dynamics and diel temperature changes (Heppell & Parker, 2018)
419 that were evaluated for both gases, as well as gas specific parameters, such as the respiratory
420 quotient to convert O₂ fluxes to CO₂ equivalents and suspended particulate matter
421 concentrations (Heppell & Binley, 2016b), used as a descriptor for methane oxidation in the
422 water column. While k is parametrized in the model as described above, and thus coupled to
423 stream discharge, k values associated the lower and upper end of the observed discharge were
424 also applied to the base model to assess the sensitivity of the diel outgassing dynamics to
425 changes in gas transfer velocity.

426

427 2.8 Statistical Analysis.

428 We used linear mixed effects models with the lme4 package in R (Bates et al., 2015;
429 Pinheiro & Bates, 2000; R Core Team, 2014) to estimate the overall main effect of light,
430 season, patch type (gravel, sand, clay and vegetated sediment) or individual stream on
431 measured benthic O₂ and CH₄ exchange. For example, to isolate the overall main effect of
432 light we pooled the data for each stream and each seasonal campaign and fitted models that
433 included season and stream as random effects on the intercepts (see Tables S1 to S3). Note,
434 that the effect of patch type was not tested in the turbid clay streams as the beds were
435 homogenous, i.e., there were no vegetated patches. Similarly, we modeled the overall main
436 relationship between outgassing and discharge for CO₂ or CH₄ by pooling the data from each
437 seasonal campaign and fitting slopes and intercepts as random effects to the data for each
438 stream. In each case, nested models of varying complexity, e.g., models with random slopes
439 and intercepts *versus* random intercepts only, were compared using the Akaike Information
440 Criterion (AICc for small samples sizes) with the “MuMin” package (Barton, 2009) and final
441 parameter estimates for the most parsimonious models derived using the “emmeans” package
442 (Lenth, 2019). Where appropriate, the overall relationship in the data is visualized by plotting
443 the partial residuals from the mixed-effects model. Data with a high degree of skewness were

444 cube-root ($\sqrt[3]{}$) transformed to improve normality and to maintain the original positive and
445 negative value structure in the data (Miles et al., 2013; Zuur et al., 2009). Further details are
446 given in the Supplementary Information.

447

448 **3 Results**

449 3.1 Seasonal field campaigns

450 3.1.1 CO₂ fluxes, outgassing *versus* discharge and porewater concentrations

451 Rates of CO₂ outgassing (in mmol m⁻² h⁻¹) from the streams, quantified with floating
452 chambers, were strongly seasonal, ranging from 3.95 ± 0.63 (4.12) (mean \pm standard error
453 (median)) in spring, to 16.66 ± 2.67 (13.07) during winter (Figure 2a), while chamber-based
454 net benthic metabolism (in mmol m⁻² h⁻¹) ranged from -0.10 ± 0.51 (-0.34) on average, in
455 spring, to 0.69 ± 0.21 (0.87) in autumn (Figure 2a). Contributions of net benthic metabolism
456 to CO₂ outgassing varied among seasons, ranging from ~69% in summer, to ~22% in spring
457 and autumn, to ~8% during the winter, but represented only about a third of the estimated
458 mean annual CO₂ outgassing (Table 1). Assessments of net whole-stream metabolism (in
459 mmol m⁻² h⁻¹) using aquatic eddy covariance showed that half the reaches acted as CO₂ sinks
460 (negative net whole-stream metabolism) in spring and summer. Overall, seasonal averages
461 were negative and/or carbon neutral (-0.53 and -0.02; Figure 2a), being -20% and -30% of the
462 CO₂ outgassing rates, respectively, on average. In contrast, in autumn and winter the net
463 whole-stream metabolism was positive, but comprised only 25% (2.42 mmol m⁻² h⁻¹) and
464 17% (1.81 mmol m⁻² h⁻¹) of seasonal total outgassing of all streams, respectively. Outgassing
465 of CO₂ was not correlated with the observed rates of net benthic or whole-stream metabolism,
466 but was almost linearly proportional to stream discharge and baseflow (discharge normalized
467 by the respective sub-catchment areas, power-law exponent 0.84 *versus* 1; Figure 2b, Table
468 S1). Outgassing was maximal in autumn and winter under high discharge and lowest in
469 summer. Porewater concentrations of CO₂ in the streambed and riparian soils of gaining
470 reaches were comparable (Figure 2e). Overall, on the clay, the net benthic metabolism could
471 account for 70% of the outgassed CO₂ in spring and all of CO₂ outgassing in summer
472 (average of Priors and Sem sites in Table 1). In contrast, on the Chalk and Greensand, net
473 benthic metabolism in spring and summer could only account on average for 8 to 10% of CO₂
474 outgassing at these sites, respectively (Table 1).

475

476 3.1.2 CH₄ fluxes, outgassing *versus* discharge and porewater concentrations

477 Outgassing of CH₄ (in mmol m⁻² h⁻¹; mean ± se (median)) to the atmosphere ranged
478 from 0.04 ± 0.02 (0.03) during summer, to 0.07 ± 0.03 (0.05) during autumn (Figure 2c).
479 Chamber-based release of CH₄ from the sediments ranged from 0.37 ± 0.13 (0.23) in autumn,
480 to 0.82 ± 0.24 (0.65) in winter (Figure 2c) and was up to 50 times higher than CH₄ outgassing
481 (Figure 2c). The release of CH₄ from the streambed was also not correlated with CH₄
482 outgassing and revealed a non-linear relationship to normalized stream discharge (Figure 2d,
483 Table S2). Porewater concentrations within the streambed and in bankside riparian soils in
484 gaining reaches, were highly variable, but, overall, riparian CH₄ concentrations were four-
485 fold lower (median to median) than in the streambed (Figure 2e). The release of CH₄ from the
486 streambed (in μmol m⁻² h⁻¹) showed large variation both across streams and seasons, but,
487 overall, streambed sediments in the dark released significantly ($P < 0.001$, see Table S3)
488 more CH₄ (median 23.8) than streambed sediments in the light (median 2.11, Figure 3). The
489 only exception being the River Nadder on the Greensand, where the CH₄ release in the light
490 was 7% higher than in the dark (Figure S3). Generally, mean sediment CH₄ release,
491 quantified from our data clustering approach, was highest on clay (up to 8.18, on average
492 at night) and on sand streams (up to 18.5), with very little contribution from the Chalk gravels
493 (up 0.04) (Figure 3). In contrast, vegetated patches of both Greensand and Chalk streambeds
494 were found to be hotspots of CH₄ release (58.8).

495

496 3.2 High-resolution diel CO₂ and CH₄ outgassing in spring

497 We used high-resolution automated floating chambers to characterize diel dynamics
498 of CO₂ and CH₄ outgassing. For CO₂, mean daytime outgassing (in mmol m⁻² h⁻¹) ranged
499 from 0.54 ± 0.02 (mean ± standard error) to 13.52 ± 0.35 across the six streams, while at
500 night, outgassing was 30% higher, on average ($P = 0.036$, Figure 4a). Only 3.5% of the
501 dataset (49 values) failed our quality check ($r^2 < 0.9$). Mean outgassing of CH₄ remained
502 largely constant across the day, with no significant daytime to nighttime variability ($P =$
503 0.455; Figure 4b). Averaged daytime CH₄ outgassing (in μmol m⁻² h⁻¹) ranged from 2.10 ±
504 0.05 to 56.82 ± 1.15. Increases in CO₂ outgassing at night tended to be greatest in streams on
505 the Greensand and Chalk, where GPP tends to be the highest (e.g., average reach-scale
506 estimates determined in 2013-14; Rovelli et al., 2017) despite its intrinsic temporal variability
507 (see Hall, 2016; and references therein), and lowest on the more turbid clay streams, where

508 GPP also tends to be the lowest (Figure 4c). Discharge values (51 measurements, 3.5% of
509 total) were mostly concomitant with those for CO₂.

510 Out of the total 1416 high-resolution chamber measurements, we only observed 21
511 ebullition events (i.e., 1.5%), and almost all exclusively at Priors (18 events, 86% of all
512 events) on the clay. During these events, contributions from ebullition to total CH₄ outgassing
513 (ebullition + diffusion), expressed as a percentage, was 13.5%, on average, ranging from no
514 measured increase (33% of ebullition events) to 43% (1 event) and 73% (1 event) at River
515 Ebble and West Avon, respectively. At River Nadder and Priors, the increase was found to be
516 only 3% (1 event) and 9% (average of 18 events), respectively (Figure S9). Overall,
517 ebullition had a very marginal effect on mean day and night CH₄ outgassing, with 0.7% at
518 Priors, 0.5% at the Ebble, 0.3% at West Avon and a negligible 0.03% at the Nadder.

519 3.3 Methane oxidation potential and in-stream CH₄ turnover

520 Concentrations of suspended particulate matter ranged from 11 mg L⁻¹ to 16 mg L⁻¹ in
521 Greensand streams in summer, up to 501 mg L⁻¹ on the clay in autumn (Figure S5c). On
522 average, suspended particulate matter was lowest on the Chalk (River Ebble; 88 ± 20 mg L⁻¹,
523 mean ± standard error), intermediate on the Greensand (126 ± 58 and 129 ± 72 mg L⁻¹ for
524 River Nadder and West Avon, respectively) and highest on the clay (River Sem; 287 ± 91 mg
525 L⁻¹). Laboratory-determined rates of potential methane oxidation ranged from 1.35 nmol L⁻¹
526 h⁻¹ for negligible (~0 mg L⁻¹) suspended particulate matter in the Greensand West Avon, to
527 32.22 nmol L⁻¹ h⁻¹ in the clay-based River Sem for 52 mg L⁻¹ suspended particulate matter,
528 with an overall robust correlation between methane oxidation and suspended particulate
529 matter across all streams ($P < 0.001$, Figure S5). Rates of methane oxidation normalized to
530 suspended particulate matter (in nmol mg⁻¹ h⁻¹) were 0.98 ± 0.44, on average, and highest for
531 Greensand streams (1.38 to 2.52) and lowest for the Chalk River Wyllye (0.19). For the clay
532 streams, methane oxidation activity was in between, although at the lower end (0.37 to 0.45).
533 Concentrations of CH₄, normalized to suspended particulate matter, ranged from 3.82 to
534 53.64 nmol mg⁻¹, with no clear trend across geologies. Turnover of CH₄ in the water column
535 via biological methane oxidation, quantified as R_{KCH_4} , ranged from <0.01 to 0.22 h⁻¹ and was
536 0.04 ± 0.01 (0.01) (mean ± standard error (median)), on average (Figure 4d). In contrast,
537 turnover of CH₄ driven by gas transfer out of the streams (K_{CH_4}) and flow driven dilution

538 (K_{flow}), were both substantially higher at 0.26 ± 0.02 (0.25) and 3.98 ± 0.57 (4.00) h^{-1} ,
539 respectively (Figure 4d).

540 3.4 Reach-scale mass balance modeling

541 3.4.1 Mean benthic CH_4 fluxes

542 The model was run with the mean benthic CH_4 fluxes from our logarithmic transformation
543 and clustering approach. Mean estimates for average night and day fluxes (in $\mu\text{mol m}^{-2} \text{h}^{-1}$)
544 were highest for the vegetated patches (night 58.78 and day 19.51) and lower, but still
545 elevated, for the sandy patches (18.49 and 7.43) and for the clay streambed (8.18 and 4.32),
546 respectively. For the gravel patch type, fluxes were strongly reduced at night (average 0.04)
547 and turned negative, i.e. becoming sinks for CH_4 during the day (average -0.25).

548 3.4.2 Modelled reaches

549 Our model was applied to three of the reaches, representing the Chalk (River Wylye),
550 Greensand (River Nadder) and clay (River Sem) during the summer. These sites were
551 selected because they have been more extensively investigated with regards to O_2 fluxes (see
552 Rovelli et al., 2017) which are used here to drive in-stream CO_2 dynamics. The model was
553 run until day and night CO_2 and CH_4 concentrations reached steady-state and constant
554 outgassing rates were achieved, which is illustrated in Figure 5b for the River Wylye.
555 Overall, the model was able to reproduce the magnitude of observed CO_2 and CH_4 night
556 outgassing rates at all three sites (Figure 5c). In terms of actual deviation from the observed
557 day and night difference in outgassing, the model matched the dynamics in the Chalk and
558 clay reaches (<3% deviation), but was found to underestimate diel outgassing in the
559 Greensand reach by 20% (Figure 5d). In contrast, for CH_4 , the Greensand model showed
560 good agreement with the observations with only 4 % deviation. On the Chalk, the model
561 could not initially reproduce the observed diel trends when contributions from the vegetated
562 patches were scaled to their spatial coverage (51.5% of the reach), but was found to match the
563 observations when a smaller fraction of this area (25%) was considered as a hotspot for CH_4
564 release. For the clay site, the model suggested a 4% difference between day and night
565 outgassing of CH_4 which was at odds with the observed 21%. Due to the disproportionately

566 high standard error around the measured nighttime outgassing rate, this 21% difference was
567 found to be not significant.

568 Modelling showed that, within the observed range of discharge, diel differences in
569 CO₂ outgassing varied by up to 17% during the extremes of low flow and high flow (Table
570 S4). Discharge, however, had a weaker effect (~6 % offset) on CH₄ than CO₂ at all sites.
571 Temperature changes, exemplified by a 10% shift in mean temperature towards both lower
572 nighttime and higher daytime averages, were found to change modelled outgassing for both
573 gases by 6% to 9%. Changing the respiratory quotient from 0.8:1 to 1.2:1 (O₂:CO₂
574 equivalents), had only a minor effect (<7%). Small changes in suspended particulate matter
575 (10% to 20%) also had very little effect (<1%) on modelled CH₄ outgassing, while peak
576 (seasonal or annual) suspended particulate matter concentrations drove changes comparable
577 in magnitude to those associated with changes in discharge. For the more turbid water of the
578 clay and Greensand sites (River Sem and Nadder respectively) we also found that, under low
579 flows, concentrations of suspended particulate matter ~240 mg L⁻¹, well below peak values,
580 could potentially drive methane oxidation rates comparable in magnitude to the overall
581 outgassing and effectively reducing daytime outgassing to 0 (Table S4). Values of *k* showed
582 reduced variability across all three modeled reaches, increasing by about 50% between low
583 discharge and high discharge conditions. When decoupled from discharge, such changes
584 drove increases or decreases in outgassing that were on average 14% to 16%, for CH₄ and
585 CO₂ across the sites. As the magnitude of both day and night outgassing are proportionally
586 affected, the initial day-to-night ratio remained unchanged (Table S4).

587

588 **4 Discussion**

589 4.1 In-stream contributions to seasonal outgassing

590 The combined dataset from our array of flux measurement techniques revealed a
591 marked difference in the magnitude of CO₂ and CH₄ outgassing compared to what could be
592 accounted for by in-stream metabolism (Figure 2, Table 1). Given that our flux techniques
593 integrate contrasting footprint areas, from patch-scale to km-long stream stretches, these
594 results must be considered within a spatial context, in term of representativeness of in-stream
595 dynamics. In Rovelli et al. (2018) we have shown for two of the investigated streams that
596 benthic and whole-stream metabolism from based on aquatic eddy covariance were
597 representative enough of in-stream dynamics to be combined with km-long assessments of O₂
598 water-air gas exchange (single station approach) to close the local O₂ budget regardless of

599 their spatial differences. As the same considerations for site selections was applied to each
600 site, here and in Rovelli et al. (2017,2018), one could reasonably assume that in-stream
601 dynamics were adequately represented within those measurements. Outgassing of CO₂ was
602 strongly proportional to stream discharge (Figure 2b) indicating that catchment processes in
603 the form of groundwater and soil water inputs are an important overall controlling factor
604 (Butman & Raymond, 2011; Marx et al., 2017). The relative contributions of each input have
605 not been quantified in this study but soil-derived CO₂ inputs from shallow lateral subsurface
606 flows are likely to be relatively more important at the clay sites compared to the
607 groundwater-fed streams on the Chalk and Greensand. Given the high proportion of
608 groundwater-derived baseflow throughout the year in the Chalk sites (90%, exemplified in
609 Figure S1c) it seems likely that, for these streams, CO₂ derived from deeper groundwater
610 sources dominate inputs. The lack of a similar relationship for CH₄ outgassing suggests other
611 factors contribute, including local streambed sources of CH₄, that we know have a high
612 potential to produce CH₄ (Bodmer et al., 2020; Crawford & Stanley, 2016; Romeijn et al.,
613 2019; Sanders et al., 2007; Schindler & Krabbenhoft, 1998; Shelley et al., 2015). Further
614 inputs might arise also from proportional changes in the upstream contributions of CH₄ in
615 different flow pathways (e.g., under baseflow and quickflow). Although CO₂ outgassing
616 could be predicted much better by discharge than by net benthic metabolism, all the
617 streambeds were typically net heterotrophic (with the exception, in spring, of the Ebble on the
618 Chalk and the Nadder on the Greensand), acting as sources of both CO₂ and CH₄ to the
619 streams (Figure 2). In spring and summer, half the reaches acted as CO₂ sinks (negative net
620 whole-stream metabolism, illustrating the important control that photosynthetic activity
621 exerts on carbon dynamics in these lowland, headwater streams (Figure 2, Table 1). During
622 autumn and winter, net whole-stream metabolism was positive, but still more than 80% of the
623 CO₂ outgassing was attributable to transport in from the catchment. Thus, even though
624 overall the streambeds act as CO₂ sources (yearly median 0.57 mmol m⁻² d⁻¹), the majority of
625 CO₂ appears catchment-derived (see Hotchkiss et al., 2015), but seasonal dynamics in CO₂
626 outgassing are modulated by in-stream metabolism.

627 4.2 Modulation of outgassing from catchment geology

628 In addition to the broad, overall patterns in CO₂ outgassing and discharge, i.e.,
629 averages across all six streams in Figure 2, there was also variation in sources and sinks in
630 relation to underlying catchment geology. Elsewhere, we have shown that dynamics in net

631 whole-stream metabolism were distinctive across these geologies, with clay reaches largely
632 representing biological sources of CO₂, Chalk reaches typically representing CO₂ sinks, and
633 the Greensand shifting from sinks for CO₂ in spring, to sources throughout the rest of the year
634 (Rovelli et al., 2017). On the clay, we found that a large portion of CO₂ outgassing in spring
635 could be accounted by the net benthic metabolism, while in summer, the totality of outgassed
636 CO₂ could be attributed to streambed metabolism. In contrast, streambed metabolism on the
637 Chalk and Greensand could only account for up to 13% of the total outgassing (Table 1),
638 indicating that while carbonate-rich groundwater inputs are significant sources of CO₂ to
639 groundwater-fed streams on Chalk and Greensand (Gallois & Owen, 2018), such contribution
640 is minimal in impermeable clay streams.

641 4.3 Diel dynamics

642 Our high-temporal-resolution measurements (spring 2015) showed a clear decrease in CO₂
643 outgassing during the day across all streams. Such a diel pattern is consistent with the
644 modulation of CO₂ concentration from in-stream metabolism (i.e., streambed, water column
645 and riparian zone) which offsets CO₂ concentrations towards higher values *via* respiration at
646 night and towards lower values *via* net primary production during the day (Herreid et al.,
647 2020; Hotchkiss et al., 2015; Lynch et al., 2010; Rocher-Ros et al., 2020). Our mean CO₂
648 outgassing rates were consistent with those reported by Attermeyer et al. (2021) for a
649 collection of 34 European rivers (median up to 25.6 mmol m⁻² h⁻¹) including 13 headwaters
650 (stream order 1-3; median up to 20.5 mmol m⁻² h⁻¹), where drifting flux chambers were used
651 on a seasonal basis. Our results are also in line with their overall reported increase of 39%
652 and 24% between midday and nighttime CO₂ outgassing (all seasons combined and
653 summertime only respectively). Comparable findings were also reported from empirical
654 models (e.g., Gómez-Gener et al., (2021)), where the authors reported an overall 27% diel
655 difference in outgassing based on long-term monitoring of over 66 streams worldwide.

656 For CH₄, the magnitude of our chamber-based estimates of outgassing are
657 representative of the global averages for headwaters presented by Stanley et al. (2016) based
658 on a large (n=205) database of headwater streams, which includes estimates for other lowland
659 headwaters in temperate climates (e.g., Hlaváčová et al., 2006). In contrast to our
660 observations for CO₂, diel CH₄ outgassing remained constant (Figure 4) and was thus at odds
661 with the approximate doubling of CH₄ released from the sediments between dark and light
662 chambers (Figure 3). This suggests that before being outgassed through re-aeration, CH₄

663 released from strong sources such as vegetated sediments could: (i) be diluted within the
664 water column by water with a lower concentration of CH₄ (immediate surroundings and
665 upstream); and/or (ii) be oxidized in the water column, especially in the more turbid streams
666 on the clay and Greensand (Rovelli et al., 2017; Sawakuchi et al., 2016). We tested these
667 hypotheses by comparing the turnover time for CH₄ in the stream associated with outgassing
668 (K_{CH_4}), with turnover due to methane oxidation in the water column (Rk_{CH_4}) and flow-driven
669 dilution (K_{flow}). A ratio of Rk_{CH_4} to K_{CH_4} higher than 1, for example, would indicate that
670 methane oxidation plays a major role modulating CH₄ concentration changes in the water
671 column. As shown in Figure 5, however, the potential for CH₄ to be removed by methane
672 oxidation in the water column is trivial compared to outgassing through re-aeration. Here the
673 ratio was consistently < 0.2 (median) and would only approach 1 when suspended particulate
674 matter concentrations exceed 300 to 400 mg L⁻¹, which only occurred during brief periods of
675 intense rainfall during our study (see Figures S1 and S5). The influence of methane oxidation
676 in the water column would be even lower for CH₄ transported rapidly through the water
677 column by ebullition (McGinnis et al., 2016). In this study, our analysis of the high-resolution
678 outgassing dataset showed very little evidence of ebullition events, and their effect on the
679 overall outgassing rates was found to be minimal (Figure S9). The likely reason for this is
680 that porewater CH₄ concentrations in our streambed sediments were just too low for
681 widespread development of CH₄ bubbles in the sediment (median CH₄ concentrations =
682 0.718 μmol L⁻¹, Figure 1e, in our streambeds c.f. 1000s μmol L⁻¹ CH₄ reported by McGinnis
683 et al. (2016) for a stream where ebullition was identified as the main driver of CH₄
684 outgassing). In the absence of strong ebullition, the turnover of CH₄ in the water column will
685 likely be determined by the interplay of K_{CH_4} and K_{flow} . Across sites, the ratio of K_{flow} to K_{CH_4}
686 was, on average, 15 to 1, indicating that dilution by stream flow likely impresses the
687 dominant control on in-stream CH₄ concentrations and their temporal variability.

688 To further rationalize the differences that we observed between the day and night
689 outgassing rates for CH₄ and CO₂, we applied our mass-balance model to three reaches,
690 ranging from a fast-flowing highly-productive clear-water stream on the Chalk (River Wyllye)
691 to a slow-flowing turbid stream on the clay (River Sem), with the River Nadder on the
692 Greensand representing an intermediate system. On the Chalk, despite large CO₂ import from
693 the groundwater-fed catchment and enhanced dilution from high flow, we expected in-stream
694 metabolism (i.e., net benthic and whole-stream metabolism) to exert a clear modulation on
695 diel variability in CO₂ outgassing. On the Clay, conversely, we expected to have the best

696 chance of detecting diel changes in CH₄ outgassing, as here we observed strong streambed
697 CH₄ release in combination with the highest ratio of Rk_{CH_4} to K_{flow} of all sites.

698 Despite the recognized simplicity of our model (see Methods), we were mostly able to
699 reproduce the contrasting diel patterns that we observed for CO₂ and CH₄ in the field (Figure
700 5c,d), thus further validating the representativeness of our assessment of in-stream
701 metabolism. For CO₂, the largest deviation from the observed outgassing rates was found on
702 the Greensand; likely a result of under-representation of the heterogeneity of the sand patch
703 type. Whilst the majority of CO₂ in the stream water is transported in from the catchment
704 (Butman & Raymond, 2011; Hotchkiss et al., 2015), primary production, and respiration at
705 the reach scale during the summer months, significantly split the resulting CO₂ outgassing
706 between night and day (Figure 4, Figure 5). Later in the year, in autumn and/or winter, these
707 streams turn into biological sources of CO₂, i.e., positive net whole-stream metabolism (see
708 Rovelli et al., 2017) likely making decreases in daytime CO₂ concentration from gross
709 primary production less pronounced, thus dampening the overall diel CO₂ dynamics.

710 In contrast, CH₄ present in the stream water is predominantly produced in the
711 streambed, with the magnitude of production depending on sediment type (Jones &
712 Mulholland, 1998a; Shelley et al., 2015) (Figure 3a). Release of CH₄ from a streambed can
713 be less during the day, most likely due to diel changes in microphytobenthic O₂ production on
714 the immediate streambed (Fenchel & Glud, 2000) and deeper hyporheic, temperature-
715 modulated microbial metabolism (e.g., Mächler et al., 2013). The main challenge when
716 quantifying CH₄ benthic release at the reach scale remains the integration of the contributions
717 from hotspots, e.g. fine sediment accumulated under vegetation (see Sanders et al., 2007).
718 Such hotspots (such as *Ranunculus* patches in chalk rivers) are heterogeneous in terms of
719 both sediment depth and areal extent, and change in shape and volume with the seasonal
720 growth and die-back of vegetation (Cotton et al., 2006; Sanders et al., 2007). On the Chalk
721 River Wyllye, we found that only 25% of the contributions from the observed vegetated patch
722 area were needed to provide a good model fit to our observational data, with higher
723 percentage contributions resulting in an over-estimate of reach-scale benthic CH₄ release.
724 This suggests that these fine-sediment patches might be more heterogeneous in terms of CH₄
725 release than we were able to resolve with our patch-scale measurements.

726 In general, we found that once released into the water column, the overall sediment
727 CH₄ signal is diluted and dissipated by stream flow, rather than by biologically mediated

728 methane oxidation in the water column; and the resulting space and time integrated CH₄
729 outgassing rates to the atmosphere remain comparatively constant between day and night
730 (Figure 4, Figure 5). It should also be noted that the highest R_{KCH_4} values, driven by the
731 highest methane oxidation activity, occurred during periods of intense rainfall, when
732 suspended particulate matter concentrations were high and discharge elevated above
733 baseflow. As a result, K_{flow} and likely K_{CH_4} would both be enhanced, with the overall effect of
734 methane oxidation on CH₄ dynamics being even further dampened, as shown by our model
735 (see Table S4). In contrast, regions of reduced flows within a stream (e.g., pools and marginal
736 regions) or periods of strongly reduced flow (e.g., during summertime droughts) would
737 enhance R_{KCH_4} locally and thus increase the importance of methane oxidation to water
738 column CH₄ dynamics. In terms of emissions, however, such conditions would also reduce
739 re-aeration (K_{CH_4}), and the concentration of CH₄ in the water column, thus strongly limiting
740 the overall outgassing of CH₄ from the reach, as illustrated in our model for the more turbid
741 streams (clay and Greensand, Table S4).

742

743 **5 Conclusions**

744 Here we have characterized distinct biophysical controls on the final outgassing of
745 CO₂ and CH₄ from headwater streams in lowland catchments. Outgassed CO₂ is principally
746 controlled by hydrology – tempered by season and whole stream metabolism – stressing the
747 importance of the connection between terrestrial and freshwater ecosystems with regard to
748 carbon cycling. In contrast, outgassed CH₄ is principally stream borne and, once released
749 from sediment, that CH₄ passes relatively unimpeded by biology in the water column, with
750 dilution largely governing the final integrated magnitude of CH₄ outgassing. Our
751 observations have characterized distinct biophysical controls on the two carbon gases and
752 incorporating the intense carbon cycling of headwater streams into the global carbon cycle
753 will require distinct parameterizations for each carbon gas in Earth system models.

754

755 **Acknowledgments**

756

757 This study was financially supported through the Natural Environment Research
758 Council (NERC) Macronutrient Cycles Programme (grant numbers NE/J012106/1, MT, and

759 NE/J011738/1, AB), the German Science Foundation (grant RO 5921/1-1, LR). This work
760 was funded by HADES-ERC Advanced Grant (No. 669947), the FNU-7014-00078 grant and
761 the Danish National Research Foundation through the Danish Center for Hadal Research,
762 HADAL (No. DNRF145) awarded to R.N. Glud. We acknowledge the land owners for
763 allowing us access to the streams and thanks E. Malone, A. Jones, S. Warren, I. Sanders, F.
764 Shelley and V. Warren for help with sample collection and preparation. Data presented in this
765 work are available from NERC Environmental Information Data Centre.

766

767 **Additional information**

768 Supplementary information is available in the online version of the paper.

769

770 **References**

- 771 Allen, D. J., Darling, W. G., Davies, J., Newell, A. J., Goody, D. C., & Collins, A. L. (2014). Groundwater
772 conceptual models: implications for evaluating diffuse pollution mitigation measures. *Quarterly Journal*
773 *of Engineering Geology and Hydrogeology*, 47(1), 65–80. <https://doi.org/10.1144/qjgegh2013-043>
- 774 Attard, K. M., Stahl, H., Kamenos, N. A., Turner, G., Burdett, H. L., & Glud, R. N. (2015). Benthic oxygen
775 exchange in a live coralline algal bed and an adjacent sandy habitat: an eddy covariance study. *Marine*
776 *Ecology Progress Series*, 535, 99–115. <https://doi.org/10.3354/meps11413>
- 777 Attermeyer, K., Casas-Ruiz, J. P., Fuss, T., Pastor, A., Cauvy-Fraunié, S., Sheath, D., et al. (2021). Carbon
778 dioxide fluxes increase from day to night across European streams. *Communications Earth &*
779 *Environment*, 2(1), 118. <https://doi.org/10.1038/s43247-021-00192-w>
- 780 Barton, K. (2009). Multi-model inference. R Package Version 1.43.15. Retrieved from [http://r-forge.r-](http://r-forge.r-project.org/projects/mumin/)
781 [project.org/projects/mumin/](http://r-forge.r-project.org/projects/mumin/)
- 782 Bastviken, D., Tranvik, L. J., Downing, J. A., Crill, P. M., & Enrich-Prast, A. (2011). Freshwater Methane
783 Emissions Offset the Continental Carbon Sink. *Science*, 331(6013), 50–50.
784 <https://doi.org/10.1126/science.1196808>
- 785 Bastviken, D., Sundgren, I., Natchimuthu, S., Reyier, H., & Gålfalk, M. (2015). Technical Note: Cost-efficient
786 approaches to measure carbon dioxide (CO₂) fluxes and concentrations in terrestrial and aquatic
787 environments using mini loggers. *Biogeosciences*, 12(12), 3849–3859. [https://doi.org/10.5194/bg-12-](https://doi.org/10.5194/bg-12-3849-2015)
788 [3849-2015](https://doi.org/10.5194/bg-12-3849-2015)
- 789 Bates, D., Mächler, M., Bolker, B. M., & Walker, S. C. (2015). Fitting linear mixed-effects models using lme4.
790 *Journal of Statistical Software*. <https://doi.org/10.18637/jss.v067.i01>
- 791 Battin, T. J., Luysaert, S., Kaplan, L. A., Aufdenkampe, A. K., Richter, A., & Tranvik, L. J. (2009). The
792 boundless carbon cycle. *Nature Geoscience*, 2(9), 598–600. <https://doi.org/10.1038/ngeo618>
- 793 Berg, P., & Pace, M. L. (2017). Continuous measurement of air–water gas exchange by underwater eddy
794 covariance. *Biogeosciences*, 14(23), 5595–5606. <https://doi.org/10.5194/bg-14-5595-2017>
- 795 Berg, P., Roy, H., Janssen, F., Meyer, V., Jorgensen, B. B., Huettel, M., & de Beer, D. (2003). Oxygen uptake
796 by aquatic sediments measured with a novel non-invasive eddy-correlation technique. *Marine Ecology*
797 *Progress Series*, 261, 75–83. <https://doi.org/10.3354/meps261075>
- 798 Berg, P., Roy, H., & Wiberg, P. L. (2007). Eddy correlation flux measurements: The sediment surface area that
799 contributes to the flux. *Limnology and Oceanography*, 52(4), 1672–1684.
800 <https://doi.org/10.4319/lo.2007.52.4.1672>
- 801 Bodmer, P., Wilkinson, J., & Lorke, A. (2020). Sediment Properties Drive Spatial Variability of Potential
802 Methane Production and Oxidation in Small Streams. *Journal of Geophysical Research: Biogeosciences*,
803 125(1). <https://doi.org/10.1029/2019JG005213>
- 804 Bristow, C. R., Barton, C. M., Westhead, R. K., Freshney, E. C., Cox, B. M., & Woods, M. A. (1999). *The*
805 *Wincanton district - a concise account of the geology. The Wincanton district - a concise account of the*
806 *geology. Memoir for 1:50 000 Geological Sheet 297 (England and Wales).*
- 807 Butman, D., & Raymond, P. A. (2011). Significant efflux of carbon dioxide from streams and rivers in the
808 United States. *Nature Geoscience*, 4(12), 839–842. <https://doi.org/10.1038/ngeo1294>
- 809 Ciais, P., Sabine, C., Bala, G., Bopp, L., Brovkin, V., Canadell, J., et al. (2013). Carbon and Other
810 Biogeochemical Cycles. In Intergovernmental Panel on Climate Change (Ed.), *Climate Change 2013 -*
811 *The Physical Science Basis* (pp. 465–570). Cambridge: Cambridge University Press.
812 <https://doi.org/10.1017/CBO9781107415324.015>
- 813 Cole, J. J., Prairie, Y. T., Caraco, N. F., McDowell, W. H., Tranvik, L. J., Striegl, R. G., et al. (2007). Plumbing
814 the global carbon cycle: Integrating inland waters into the terrestrial carbon budget. *Ecosystems*, 10(1),
815 171–184. <https://doi.org/10.1007/s10021-006-9013-8>
- 816 Cotton, J. A., Wharton, G., Bass, J. A. B., Heppell, C. M., & Wotton, R. S. (2006). The effects of seasonal
817 changes to in-stream vegetation cover on patterns of flow and accumulation of sediment. *Geomorphology*,
818 77(3–4), 320–334. <https://doi.org/10.1016/j.geomorph.2006.01.010>
- 819 Crawford, J. T., & Stanley, E. H. (2016). Controls on methane concentrations and fluxes in streams draining
820 human-dominated landscapes. *Ecological Applications*, 26(5), 1581–1591. [https://doi.org/10.1890/15-](https://doi.org/10.1890/15-1330)
821 [1330](https://doi.org/10.1890/15-1330)
- 822 Dalsgaard, T. (ed), Nielsen, L. P., Brotos, V., Viaroli, P., Underwood, G., Nedwell, D. B., et al. (2000). *Protocol*
823 *handbook for NICE-Nitrogen Cycling in Estuaries: a project under the EU research programme: Marine*
824 *Science and Technology (Mast III). National Environmental Research Institute.*
- 825 Fenchel, T., & Glud, R. N. (2000). Benthic primary production and O₂-CO₂ dynamics in a shallow-water
826 sediment: Spatial and temporal heterogeneity. *Ophelia*, 53(2), 159–171.
827 <https://doi.org/10.1080/00785236.2000.10409446>
- 828 Gallois, R., & Owen, H. (2018). The stratigraphy of the mid Cretaceous (Albian) Upper Greensand Formation

- 829 of the Wessex Basin and South West England, UK. *Acta Geologica Polonica*, 68(2), 161–180.
 830 <https://doi.org/10.1515/agp-2018-0003>
- 831 Glud, R. N. (2008). Oxygen dynamics of marine sediments. *Marine Biology Research*, 4(4), 243–289.
 832 <https://doi.org/10.1080/17451000801888726>
- 833 Gómez-Gener, L., Rocher-Ros, G., Battin, T., Cohen, M. J., Dalmagro, H. J., Dinsmore, K. J., et al. (2021).
 834 Global carbon dioxide efflux from rivers enhanced by high nocturnal emissions. *Nature Geoscience*,
 835 14(5), 289–294. <https://doi.org/10.1038/s41561-021-00722-3>
- 836 Gurnell, A., Angold, P., & Edwards, P. (1996). Extracting information from river corridor surveys. *Applied*
 837 *Geography*, 16(1), 1–19. [https://doi.org/10.1016/0143-6228\(95\)00022-4](https://doi.org/10.1016/0143-6228(95)00022-4)
- 838 Hall, R. O. (2016). Metabolism of Streams and Rivers. In *Stream Ecosystems in a Changing Environment* (pp.
 839 151–180). Elsevier. <https://doi.org/10.1016/B978-0-12-405890-3.00004-X>
- 840 Heppell, C. M., & Binley, A. (2016a). Hampshire Avon: Vertical head gradient, saturated hydraulic
 841 conductivity and pore water chemistry data from six river reaches. *NERC Environmental Information*
 842 *Data Centre*. <https://doi.org/10.5285/d82a04ce-f04d-40b4-9750-1a2bf7dc29a3>
- 843 Heppell, C. M., & Binley, A. J. (2016b). Hampshire Avon: Daily discharge, stage and water chemistry data
 844 from four tributaries (Sem, Nadder, West Avon, Ebble). *NERC Environmental Information Data Centre*.
 845 <https://doi.org/10.5285/0dd10858-7b96-41f1-8db5-e7b4c4168af5>
- 846 Heppell, C. M., & Parker, S. J. (2018). Hampshire Avon: Dissolved oxygen data collected at one minute
 847 intervals from five river reaches. *NERC Environmental Information Data Centre*.
 848 <https://doi.org/10.5285/840228a7-40a1-4db4-ae0-a9fea2079987>
- 849 Heppell, Catherine M., Binley, A., Trimmer, M., Darch, T., Jones, A., Malone, E., et al. (2017). Hydrological
 850 controls on DOC : nitrate resource stoichiometry in a lowland, agricultural catchment, southern UK.
 851 *Hydrology and Earth System Sciences*, 21(9), 4785–4802. <https://doi.org/10.5194/hess-21-4785-2017>
- 852 Herreid, A. M., Wymore, A. S., Varner, R. K., Potter, J. D., & McDowell, W. H. (2020). Divergent Controls on
 853 Stream Greenhouse Gas Concentrations Across a Land-Use Gradient. *Ecosystems*.
 854 <https://doi.org/10.1007/s10021-020-00584-7>
- 855 Hlaváčová, E., Rulík, M., Čáp, L., & Mach, V. (2006). Greenhouse gas (CO₂, CH₄, N₂O) emissions to the
 856 atmosphere from a small lowland stream in Czech Republic. *Archiv Für Hydrobiologie*, 165(3), 339–353.
 857 <https://doi.org/10.1127/0003-9136/2006/0165-0339>
- 858 Hotchkiss, E. R., Hall Jr, R. O., Sponseller, R. A., Butman, D., Klaminder, J., Laudon, H., et al. (2015). Sources
 859 of and processes controlling CO₂ emissions change with the size of streams and rivers. *Nature*
 860 *Geoscience*, 8(9), 696–699. <https://doi.org/10.1038/ngeo2507>
- 861 Jarvie, H. P., Jürgens, M. D., Williams, R. J., Neal, C., Davies, J. J. L., Barrett, C., & White, J. (2005). Role of
 862 river bed sediments as sources and sinks of phosphorus across two major eutrophic UK river basins: the
 863 Hampshire Avon and Herefordshire Wye. *Journal of Hydrology*, 304(1–4), 51–74.
 864 <https://doi.org/10.1016/j.jhydrol.2004.10.002>
- 865 Jones, J. B., & Mulholland, P. J. (1998a). Influence of drainage basin topography and elevation on carbon
 866 dioxide and methane supersaturation of stream water. *Biogeochemistry*, 40, 57–72.
 867 <https://doi.org/10.1023/A:1005914121280>
- 868 Jones, J. B., & Mulholland, P. J. (1998b). Methane input and evasion in a hardwood forest stream: Effects of
 869 subsurface flow from shallow and deep pathways. *Limnology and Oceanography*.
 870 <https://doi.org/10.4319/lo.1998.43.6.1243>
- 871 Koopmans, D. J., & Berg, P. (2015). Stream oxygen flux and metabolism determined with the open water and
 872 aquatic eddy covariance techniques. *Limnology and Oceanography*, 60(4), 1344–1355.
 873 <https://doi.org/10.1002/lno.10103>
- 874 Lansdown, K., McKew, B. A., Whitby, C., Heppell, C. M., Dumbrell, A. J., Binley, A., et al. (2016). Importance
 875 and controls of anaerobic ammonium oxidation influenced by riverbed geology. *Nature Geosci*, 9(5), 357–
 876 360. <https://doi.org/10.1038/ngeo2684>
- 877 Lenth, R. V. (2019). Emmeans: Estimated Marginal Means, aka Least-Squares Means. R package version 1.4.5.
 878 Retrieved from <https://cran.r-project.org/web/packages/emmeans/>
- 879 Li, M., Peng, C., Zhang, K., Xu, L., Wang, J., Yang, Y., et al. (2021). Headwater stream ecosystem: an
 880 important source of greenhouse gases to the atmosphere. *Water Research*, 190, 116738.
 881 <https://doi.org/10.1016/j.watres.2020.116738>
- 882 Lorke, A., Bodmer, P., Noss, C., Alshboul, Z., Koschorreck, M., Somlai-Haase, C., et al. (2015). Technical
 883 note: drifting versus anchored flux chambers for measuring greenhouse gas emissions from running
 884 waters. *Biogeosciences*, 12(23), 7013–7024. <https://doi.org/10.5194/bg-12-7013-2015>
- 885 Lorrai, C., McGinnis, D. F., Berg, P., Brand, A., & Wuest, A. (2010). Application of Oxygen Eddy Correlation
 886 in Aquatic Systems. *Journal of Atmospheric and Oceanic Technology*, 27(9), 1533–1546.
 887 <https://doi.org/10.1175/2010JTECHO723.1>
- 888 Lynch, J. K., Beatty, C. M., Seidel, M. P., Jungst, L. J., & DeGrandpre, M. D. (2010). Controls of riverine CO₂

- 889 over an annual cycle determined using direct, high temporal resolution p CO₂ measurements. *Journal of*
 890 *Geophysical Research*, 115(G3), G03016. <https://doi.org/10.1029/2009JG001132>
- 891 Mächler, L., Brennwald, M. S., & Kipfer, R. (2013). Argon Concentration Time-Series As a Tool to Study Gas
 892 Dynamics in the Hyporheic Zone. *Environmental Science & Technology*, 47(13), 7060–7066.
 893 <https://doi.org/10.1021/es305309b>
- 894 Marx, A., Dusek, J., Jankovec, J., Sanda, M., Vogel, T., van Geldern, R., et al. (2017). A review of CO₂ and
 895 associated carbon dynamics in headwater streams: A global perspective. *Reviews of Geophysics*, 55(2),
 896 560–585. <https://doi.org/10.1002/2016RG000547>
- 897 McGinnis, D. F., Cherednichenko, S., Sommer, S., Berg, P., Rovelli, L., Schwarz, R., et al. (2011). Simple,
 898 robust eddy correlation amplifier for aquatic dissolved oxygen and hydrogen sulfide flux measurements.
 899 *Limnology and Oceanography-Methods*, 9, 340–347. <https://doi.org/10.4319/lom.2011.9.340>
- 900 McGinnis, D. F., Bilsley, N., Schmidt, M., Fietzek, P., Bodmer, P., Premke, K., et al. (2016). Deconstructing
 901 Methane Emissions from a Small Northern European River: Hydrodynamics and Temperature as Key
 902 Drivers. *Environmental Science & Technology*, 50(21), 11680–11687.
 903 <https://doi.org/10.1021/acs.est.6b03268>
- 904 Miles, B. W. J., Stokes, C. R., Vieli, A., & Cox, N. J. (2013). Rapid, climate-driven changes in outlet glaciers on
 905 the Pacific coast of East Antarctica. *Nature*. <https://doi.org/10.1038/nature12382>
- 906 Millero, F. J. (1979). The thermodynamics of the carbonate system in seawater. *Geochimica et Cosmochimica*
 907 *Acta*, 43(10), 1651–1661. [https://doi.org/10.1016/0016-7037\(79\)90184-4](https://doi.org/10.1016/0016-7037(79)90184-4)
- 908 Murniati, E., Geissler, S., & Lorke, A. (2015). Short-term and seasonal variability of oxygen fluxes at the
 909 sediment–water interface in a riverine lake. *Aquatic Sciences*, 77(2), 183–196.
 910 <https://doi.org/10.1007/s00027-014-0362-7>
- 911 Myhre, G., Shindell, D., Bréon, F., Collins, W., Fuglestedt, J., Huang, J., et al. (2013). *Anthropogenic and*
 912 *natural radiative forcing. In: Climate change 2013: the physical science basis. Contribution of working*
 913 *group I. Climate Change 2013 - The Physical Science Basis.*
- 914 Peter, H., Singer, G. A., Preiler, C., Chiffard, P., Steniczka, G., & Battin, T. J. (2014). Scales and drivers of
 915 temporal p CO₂ dynamics in an Alpine stream. *Journal of Geophysical Research: Biogeosciences*,
 916 119(6), 1078–1091. <https://doi.org/10.1002/2013JG002552>
- 917 Pinheiro, J. C., & Bates, D. M. (2000). *Mixed-Effects Models in S and S-PLUS. Mixed-Effects Models in S and*
 918 *S-PLUS.* New York: Springer-Verlag. <https://doi.org/10.1007/b98882>
- 919 Podgrajsek, E., Sahlee, E., Bastviken, D., Holst, J., Lindroth, A., Tranvik, L., & Rutgersson, A. (2014).
 920 Comparison of floating chamber and eddy covariance measurements of lake greenhouse gas fluxes.
 921 *Biogeosciences*, 11(15), 4225–4233. <https://doi.org/10.5194/bg-11-4225-2014>
- 922 R Core Team. (2014). R Core Team (2014). R: A language and environment for statistical computing. *R*
 923 *Foundation for Statistical Computing, Vienna, Austria. URL Http://Www.R-Project.Org/.*
- 924 Raymond, P. A., Zappa, C. J., Butman, D., Bott, T. L., Potter, J., Mulholland, P., et al. (2012). Scaling the gas
 925 transfer velocity and hydraulic geometry in streams and small rivers. *Limnology and Oceanography:*
 926 *Fluids and Environments*, 2(1), 41–53. <https://doi.org/10.1215/21573689-1597669>
- 927 Raymond, P. A., Hartmann, J., Lauerwald, R., Sobek, S., McDonald, C., Hoover, M., et al. (2013). Global
 928 carbon dioxide emissions from inland waters. *Nature*, 503(7476), 355–359.
 929 <https://doi.org/10.1038/nature12760>
- 930 Reiman, J., & Xu, Y. (2018). Diel Variability of pCO₂ and CO₂ Outgassing from the Lower Mississippi River:
 931 Implications for Riverine CO₂ Outgassing Estimation. *Water*, 11(1), 43.
 932 <https://doi.org/10.3390/w11010043>
- 933 Revsbech, N. P. (1989). An oxygen microelectrode with a guard cathode. *Limnology and Oceanography*, 34(2),
 934 474–478. <https://doi.org/10.4319/lo.1989.34.2.0474>
- 935 Rocher-Ros, G., Sponseller, R. A., Bergström, A., Myrstener, M., & Giesler, R. (2020). Stream metabolism
 936 controls diel patterns and evasion of CO₂ in Arctic streams. *Global Change Biology*, 26(3), 1400–1413.
 937 <https://doi.org/10.1111/gcb.14895>
- 938 Romeijn, P., Comer-Warner, S. A., Ullah, S., Hannah, D. M., & Krause, S. (2019). Streambed Organic Matter
 939 Controls on Carbon Dioxide and Methane Emissions from Streams. *Environmental Science &*
 940 *Technology*, 53(5), 2364–2374. <https://doi.org/10.1021/acs.est.8b04243>
- 941 Rovelli, L., Attard, K. M., Binley, A., Heppell, C. M., Stahl, H., Trimmer, M., & Glud, R. N. (2017). Reach-
 942 scale river metabolism across contrasting sub-catchment geologies: Effect of light and hydrology.
 943 *Limnology and Oceanography*, 62(S1), S381–S399. <https://doi.org/10.1002/lno.10619>
- 944 Rovelli, L., Attard, K. M., Heppell, C. M., Binley, A., Trimmer, M., & Glud, R. N. (2018). Headwater gas
 945 exchange quantified from O₂ mass balances at the reach scale. *Limnology and Oceanography: Methods*,
 946 16(10), 696–709. <https://doi.org/10.1002/lom3.10281>
- 947 Rovelli, L., Olde, L. A., Heppell, C. M., Binley, A., Yvon Durocher, G., Glud, R. N., & Trimmer, M. . et al.
 948 (2021a). High-resolution time series of day and night outgassing rates of carbon dioxide and methane for

- 949 six tributaries of Hampshire River Avon (UK) collected with an automated floating chamber in late spring
 950 2015. *Figshare. Dataset*. <https://doi.org/10.6084/m9.figshare.16545954.v1>
- 951 Rovelli, L., Olde, L. A., Heppell, C. M., Binley, A., Yvon Durocher, G., Glud, R. N., & Trimmer, M. (2021b).
 952 Summary data of chamber-based oxygen and methane consumption and production in the streambed and
 953 outgassing of carbon dioxide and methane to the atmosphere collected seasonally for six tributaries of
 954 Hampshire River Avon (UK) during 2013-2014. *Figshare. Dataset*.
 955 <https://doi.org/10.6084/m9.figshare.16545846.v1>
- 956 Rovelli, L. ., Attard, K. M. ., Stahl, H. ., & Glud, R. N. . (2016). Summary data of reach scale oxygen
 957 consumption and production in the streambed and in the water column at six tributaries of Hampshire
 958 River Avon collected seasonally in 2013 to 2014. *NERC Environmental Information Data Centre*.
- 959 Sanders, I. A., Heppell, C. M., Cotton, J. A., Wharton, G., Hildrew, A. G., Flowers, E. J., & Trimmer, M.
 960 (2007). Emission of methane from chalk streams has potential implications for agricultural practices.
 961 *Freshwater Biology*, 52(6), 1176–1186. <https://doi.org/10.1111/j.1365-2427.2007.01745.x>
- 962 Sawakuchi, H. O., Bastviken, D., Sawakuchi, A. O., Ward, N. D., Borges, C. D., Tsai, S. M., et al. (2016).
 963 Oxidative mitigation of aquatic methane emissions in large Amazonian rivers. *Global Change Biology*,
 964 22(3), 1075–1085. <https://doi.org/10.1111/gcb.13169>
- 965 Schindler, J. E., & Krabbenhoft, D. P. (1998). The hyporheic zone as a source of dissolved organic carbon and
 966 carbon gases to a temperate forested stream. *Biogeochemistry*, 43(2), 157–174.
 967 <https://doi.org/10.1023/A:1006005311257>
- 968 Shelley, F., Grey, J., & Trimmer, M. (2014). Widespread methanotrophic primary production in lowland chalk
 969 rivers. *Proceedings of the Royal Society B: Biological Sciences*, 281(1783), 20132854–20132854.
 970 <https://doi.org/10.1098/rspb.2013.2854>
- 971 Shelley, F., Abdullahi, F., Grey, J., & Trimmer, M. (2015). Microbial methane cycling in the bed of a chalk
 972 river: oxidation has the potential to match methanogenesis enhanced by warming. *Freshwater Biology*,
 973 60(1), 150–160. <https://doi.org/10.1111/fwb.12480>
- 974 Stanley, E. H., Casson, N. J., Christel, S. T., Crawford, J. T., Loken, L. C., & Oliver, S. K. (2016). The ecology
 975 of methane in streams and rivers: patterns, controls, and global significance. *Ecological Monographs*,
 976 86(2), 146–171. <https://doi.org/10.1890/15-1027>
- 977 Stets, E. G., Butman, D., McDonald, C. P., Stackpoole, S. M., DeGrandpre, M. D., & Striegl, R. G. (2017).
 978 Carbonate buffering and metabolic controls on carbon dioxide in rivers. *Global Biogeochemical Cycles*,
 979 31(4), 663–677. <https://doi.org/10.1002/2016GB005578>
- 980 Striegl, R. G., Dornblaser, M. M., McDonald, C. P., Rover, J. R., & Stets, E. G. (2012). Carbon dioxide and
 981 methane emissions from the Yukon River system. *Global Biogeochemical Cycles*, 26(4).
 982 <https://doi.org/10.1029/2012GB004306>
- 983 Therkildsen, M. S., & Lomstein, B. A. (1993). Seasonal variation in net benthic C-mineralization in a shallow
 984 estuary. *FEMS Microbiology Ecology*, 12(2), 131–142. [https://doi.org/10.1111/j.1574-](https://doi.org/10.1111/j.1574-6941.1993.tb00025.x)
 985 [6941.1993.tb00025.x](https://doi.org/10.1111/j.1574-6941.1993.tb00025.x)
- 986 Trimmer, M., Sanders, I. . A., & Heppell, C. . M. (2009). Carbon and nitrogen cycling in a vegetated lowland
 987 chalk river impacted by sediment. *Hydrological Processes*, 23(15), 2225–2238.
 988 <https://doi.org/10.1002/Hyp.7276>
- 989 Trimmer, M., Maanoja, S., Hildrew, A. G., Pretty, J. L., & Grey, J. (2010). Potential carbon fixation via
 990 methane oxidation in well-oxygenated river bed gravels. *Limnology and Oceanography*, 55(2), 560–568.
 991 <https://doi.org/10.4319/lo.2010.55.2.0560>
- 992 Weiss, R. F. (1974). Carbon dioxide in water and seawater: the solubility of a non-ideal gas. *Marine Chemistry*,
 993 2(3), 203–215. [https://doi.org/10.1016/0304-4203\(74\)90015-2](https://doi.org/10.1016/0304-4203(74)90015-2)
- 994 Wiesenburg, D. A., & Guinasso, N. L. (1979). Equilibrium solubilities of methane, carbon monoxide, and
 995 hydrogen in water and sea water. *Journal of Chemical & Engineering Data*, 24(4), 356–360.
 996 <https://doi.org/10.1021/je60083a006>
- 997 Yamamoto, S., Alcauskas, J. B., & Crozier, T. E. (1976). Solubility of methane in distilled water and seawater.
 998 *Journal of Chemical & Engineering Data*, 21(1), 78–80. <https://doi.org/10.1021/je60068a029>
- 999 Yu, Z., Wang, D., Li, Y., Deng, H., Hu, B., Ye, M., et al. (2017). Carbon dioxide and methane dynamics in a
 1000 human-dominated lowland coastal river network (Shanghai, China). *Journal of Geophysical Research:*
 1001 *Biogeosciences*, 122(7), 1738–1758. <https://doi.org/10.1002/2017JG003798>
- 1002 Zuur, A. F., Ieno, E. N., Walker, N., Saveliev, A. A., & Smith, G. M. (2009). *Mixed effects models and*
 1003 *extensions in ecology with R*. New York, NY: Springer New York. [https://doi.org/10.1007/978-0-387-](https://doi.org/10.1007/978-0-387-87458-6)
 1004 [87458-6](https://doi.org/10.1007/978-0-387-87458-6)
- 1005

1006 **Tables**

1007

1008 **Table 1.** Percentage of CO₂ outgassing rate (CO₂out) that could potentially be accounted for by either net
 1009 benthic metabolism (NBM) or whole-stream ecosystem metabolism (NWM). The percentages are based on flux
 1010 comparisons by season and stream, and would only equal 100% if the amount of CO₂ outgassing is matched by
 1011 that of local metabolism, i.e., NBM or NWM. Note that negative values indicate net sinks for CO₂, e.g., in the
 1012 Nadder in spring, net benthic metabolism represents the potential to reduce CO₂ outgassing by 17%.

Contributions	Season	Priors (Clay)	Sem (Clay)	Ebble (Chalk)	Wylle (Chalk)	West Avon (Greensand)	Nadder (Greensand)	Seasonal average (%)
NBM / CO ₂ out	Spring	91	46	-3	9	4	-17	22
	Summer	103	234	10	17	15	39	70
	Autumn	20	20	6	82	0	9	23
	Winter	6	19	- ^a	1	- ^a	7	8
NWM / CO ₂ out	Spring	23	6	-52	-8	22	-113	-20
	Summer	-18	115	54	390	0	26	-36
	Autumn	1	107	36	-56	- ^a	38	25
	Winter	9	29	- ^a	3	- ^a	28	17

1013 ^a: site not accessible due to flooding.

1014

1015 **Figures caption**

1016

1017 **Figure 1.** Study sites and experimental setup. (a) Map of the Hampshire River Avon showing
 1018 geology and our six study sites. Red lines indicate sub-catchment boundaries delineated by
 1019 topography. (b) Schematic of benthic chamber used to quantify benthic fluxes during the
 1020 seasonal campaigns, and photograph of a set of four chambers being deployed on the West
 1021 Avon (Greensand). (c) Schematic and photograph of floating chamber used to quantify CO₂
 1022 and CH₄ outgassing during the seasonal campaigns including the underside of the chamber,
 1023 showing the CO₂ sensor and battery pack, and a typical deployment (River Nadder on the
 1024 Greensand). (d) Schematic of the automated floating chamber setup used to quantify CO₂ and
 1025 CH₄ outgassing during the spring 2015 high-resolution campaign and the system deployed on
 1026 the River Ebble on the Chalk. (e) Schematic representation of the aquatic eddy covariance
 1027 technique and underwater photograph of a typical deployment (River Wylye on the Chalk).

1028

1029 **Figure 2.** Carbon gas sources and outgassing to the atmosphere. (a) average CO₂ outgassing
 1030 rates across all six streams ($n = 55$), for each season in comparison to net-ecosystem-
 1031 metabolism for either the benthic (NBM, $n = 21$) or whole stream (NWM, $n = 21$)
 1032 metabolism. Note that positive NBM and NWM values indicate a source of CO₂. (b) CO₂
 1033 outgassing as a function of stream discharge normalized to sub-catchment area ($n = 44$). (c)
 1034 average CH₄ outgassing rates ($n = 16$) in comparison to benthic release ($n = 30$) and (d) as for
 1035 (b), but for CH₄ outgassing and discharge ($n = 15$). Box-plots (a, c) show the median
 1036 (horizontal line), 25th and 75th percentiles and overall minimum and maximum values for
 1037 each season across all six streams. Note that CH₄ outgassing rates and sediment release were
 1038 not determined (n.d.) in spring. Scatter-plots in (b), and (d), give the partial residuals after
 1039 fitting the individual outgassing rates for each stream, in each season as a function of
 1040 discharge on each occasion (see Methods and Supplementary Information). (e) comparison
 1041 between porewater CH₄ and CO₂ in piezometers in either streambed ($n = 228$) or adjacent
 1042 riparian soils ($n = 109$) from Heppell & Binley (2016a). Values indicate the median. Chamber
 1043 data are available from Rovelli et al. (2021b).

1044

1045 **Figure 3.** Sediment methane sources. *In situ* rates of CH₄ release from streambeds were
 1046 greater in the dark ($n = 140$) than in the light ($n = 141$) and were also significantly different
 1047 between the dominant streambed patch-types (gravel, sand, vegetated. $n = 39, 72, 55$,
 1048 respectively). Note that the different patch-types were only a characteristic of the sand and
 1049 Chalk-gravel streambeds and were not measured in the clay ($n = 107$). See Figures S4 and S8
 1050 and Table S3 for statistical analysis.

1051

1052 **Figure 4** Contrasting diel changes in CO₂ and CH₄ outgassing. Outgassing of CO₂ was 27%
 1053 greater at night than during the day (a), but consistent throughout for CH₄ (b). Each point in
 1054 (a) and (b) is the average rate (in mmol m⁻² h⁻¹ ± s. e.) derived from three to four days of
 1055 continuous measurements in each of the six streams in spring, 2015, with typically 230 flux
 1056 estimates for each stream (see Figure S3; Rovelli et al. (2021a)). The black lines in (a) and
 1057 (b), give the overall gradient and the grey line a 1:1 relationship. Note that the linear
 1058 regressions were performed using the reciprocal of the standard error as weighting, to give
 1059 robust average outgassing rates, with small standard errors more weight over those with
 1060 larger standard errors. (c) the difference (Δ) between night and day outgassing rates for CO₂
 1061 (a) could partly be explained by reach-scale gross primary production (GPP_w, in mmol m⁻² h⁻¹)
 1062 in each stream (see Methods; Rovelli et al., 2017, 2018). (d) In contrast, the potential for
 1063 biology to reduce CH₄ concentrations in the water column (methane oxidation on suspended

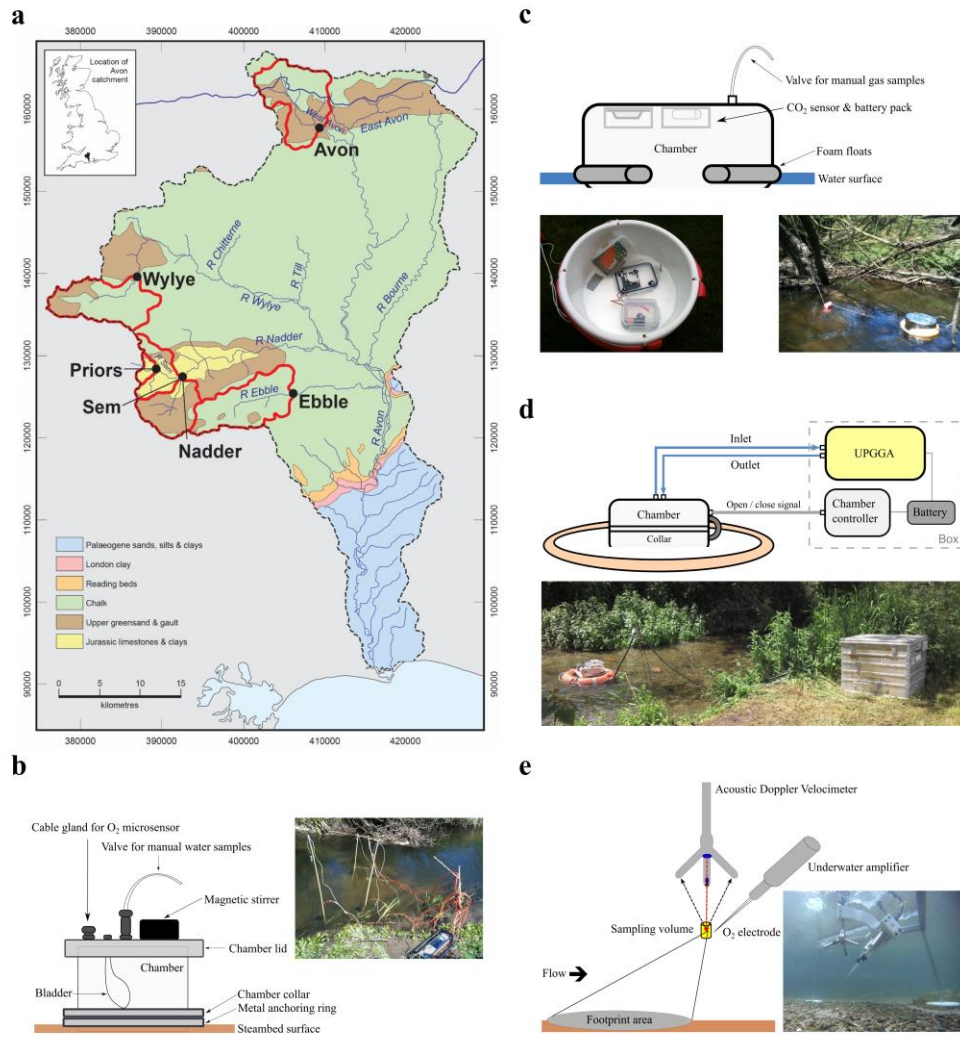
1064 particulate matter, Rk_{CH_4}) before being either outgassed (here as a reaeration constant, K_{CH_4})
1065 or diluted by the flow (K_{flow}) was negligible.

1066

1067 **Figure 5** Simple reach-scale mass-balance modeling of diel changes in CO_2 and CH_4 . (a)
1068 Changes in water column CO_2 and CH_4 are products of benthic uptake or release ($F_{\text{streambed}}$);
1069 activity in the water column ($F_{\text{water column}}$), e.g., oxidation for CH_4 and net ecosystem
1070 metabolism (NEM) for CO_2 ; outgassing at the stream surface ($F_{\text{outgassing}}$); transport from
1071 upstream (F_{in}); and advective transport downstream (F_{out}). (b) Example of development of
1072 new steady-state concentrations for CO_2 and CH_4 after the switch from day to night for the
1073 Chalk River Wylde. Background is the initial ($t = 0$) concentration in the water column
1074 ($C_{\text{background}}$), which is assumed equal to the concentration in water transported from upstream
1075 (C_{upstream}). (c) Modelled night outgassing rates *versus* observed mean outgassing rates during
1076 our high-resolution 2015 field campaign at the River Wylde (Chalk; green circles), Nadder
1077 (Greensand; blue squares) and Sem (clay; red triangles) for CO_2 (filled symbols) and CH_4
1078 (open symbols). (d) The resultant change in rate of day to night outgassing, in percentage, for
1079 each gas based on (c).

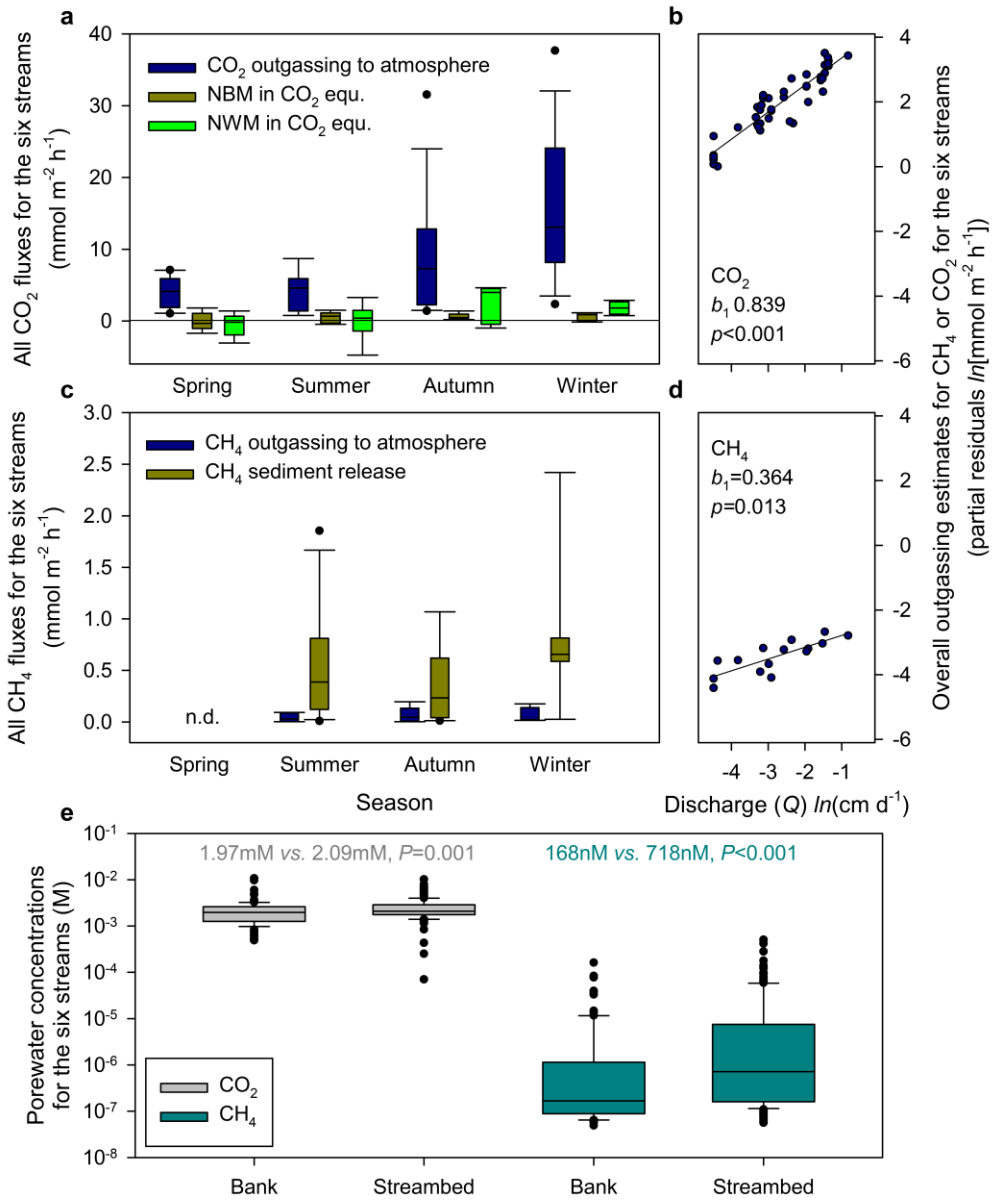
1080

1081 Figure 1

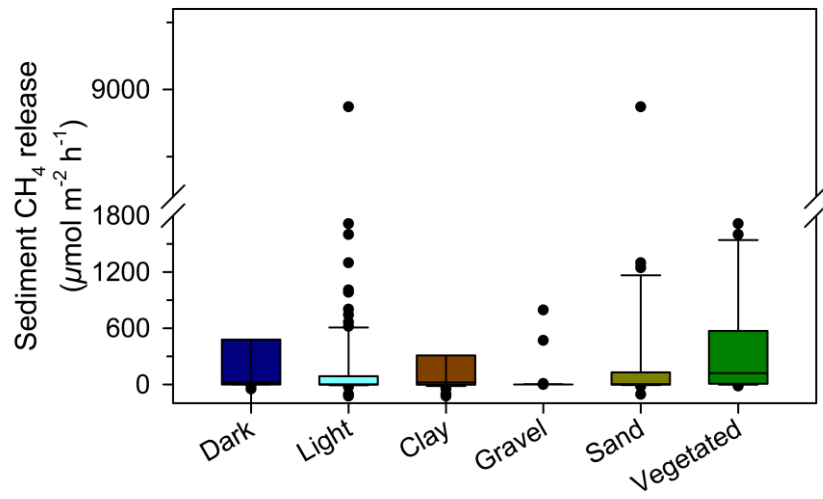


1082

1083 Figure 2

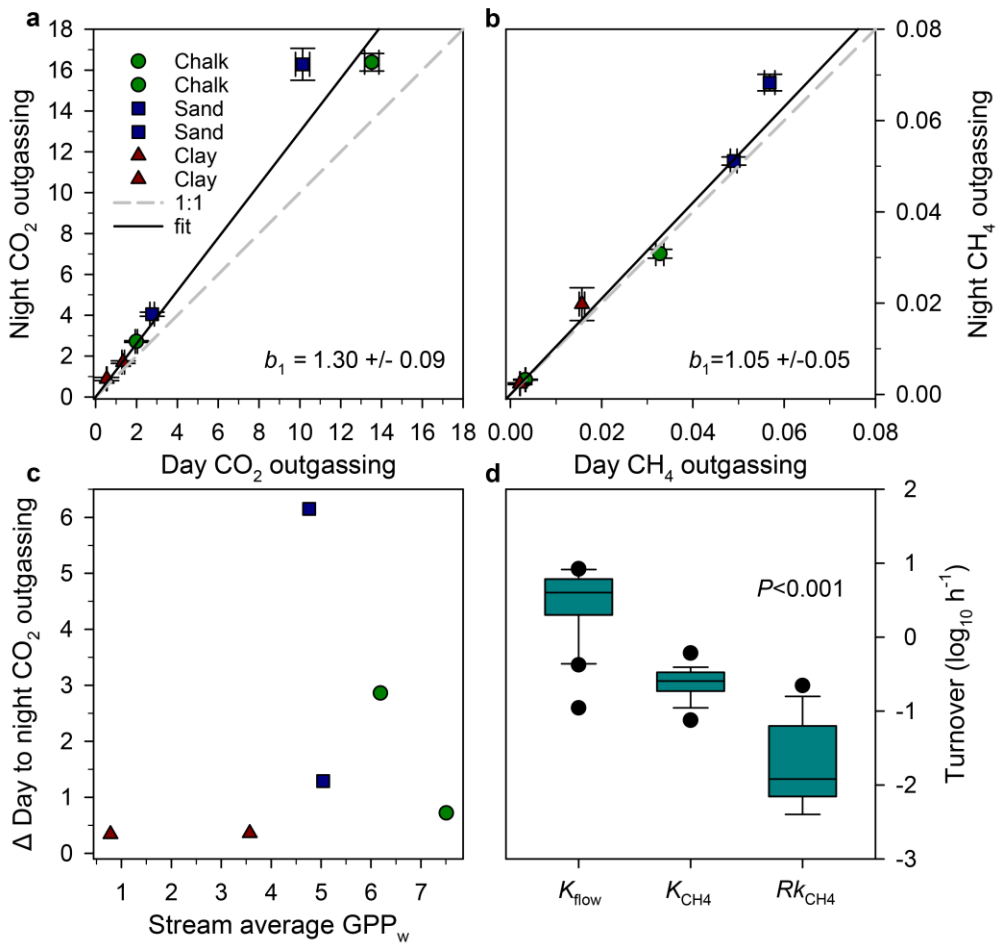


1085 Figure 3



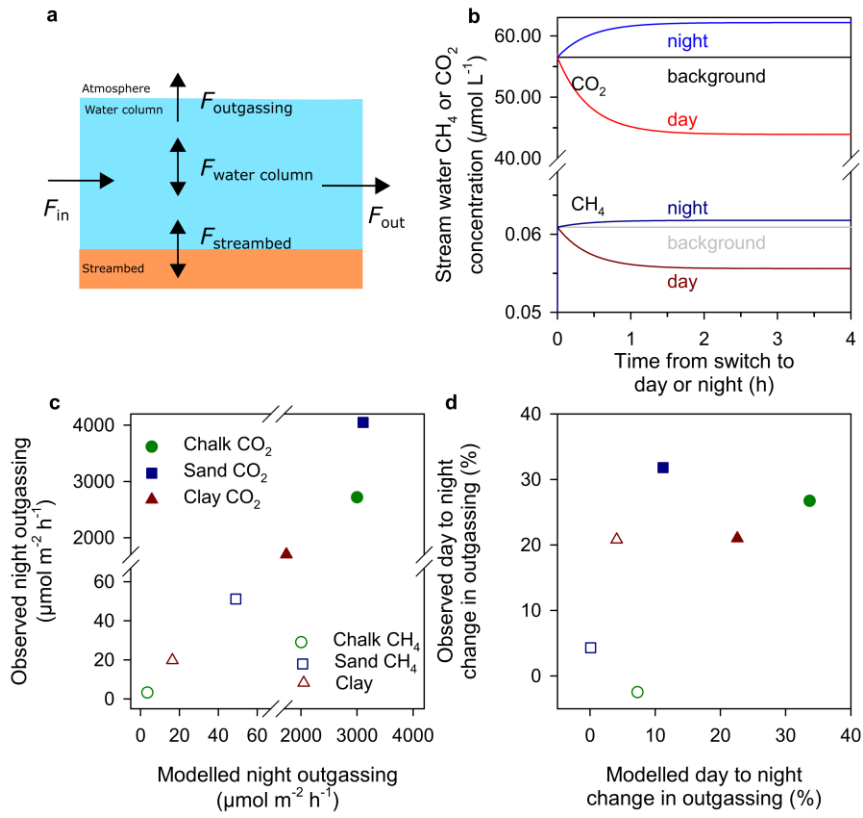
1086

1087 Figure 4



1088

1089 Figure 5



1090